Class-switch recombination occurs infrequently in germinal centers

Roco, Jonathan; Mesin, Luka; Binder, Sebastian C; Nefzger, Christian; Gonzalez-Figueroa, Paula; Canete, Pablo F; Ellyard, Julia; Shen, Qian; Robert, Philippe A; Cappello, Jean; Vohra, Harpreet; Zhang, Yang; Nowasad, Carla R; Schiepers, Arien; Corcoran, Lynn M; Toellner, Kai; Polo, Jose M; Meyer-Hermann, Michael; Victora, Gabriel D; Vinuesa, Carola G

DOI:
10.1016/j.immuni.2019.07.001

Final version manuscript of
J. A. Roco *et al.*, Class-Switch Recombination Occurs Infrequently in Germinal Centers. *Immunity* **51**, 337-350 e337 (2019).

Class Switch Recombination Occurs Infrequently in Germinal Centers

Jonathan A. Roco[1], Luka Mesin[2], Sebastian C. Binder[3], Christian Nefzger[5], Paula Gonzalez-Figueroa[1], Pablo F Canete[1], Julia Ellyard[1], Qian Shen[1], Philippe A. Robert[3], Jean Cappello[1], Harpreet Vohra[1], Yang Zhang[6], Carla R. Nowosad[2], Arien Schiepers[2], Lynn M. Corcoran[7,8], Kai-Michael Toellner[6], Jose Polo[5], Michael Meyer-Hermann[3,4], Gabriel Victora[2], and Carola G. Vinuesa[1,9].

Affiliations:

[1]*Dept of Immunology and Infectious Disease & Centre for Personalised Immunology, The John Curtin School of Medical Research, The Australian National University, Canberra, Australia.*
[2]*Laboratory of Lymphocyte Dynamics, Rockefeller University, New York, NY, 10065, USA.*
[3]*Department of Systems Immunology and Braunschweig Integrated Centre of Systems Biology, Helmholtz Centre for Infection Research, Rebenring 56, 38106 Braunschweig, Germany.*
[4]*Institute for Biochemistry, Biotechnology and Bioinformatics, Technische Universität Braunschweig, Braunschweig, Germany.*
[5]*Department of Anatomy and Developmental Biology & Australian Regenerative Medicine Institute, Monash University, Wellington Road, Clayton, VIC 3800, Australia.*
[6]*Institute of Immunology and Immunotherapy, University of Birmingham, Birmingham B15 2TT, UK.*
[7]*Molecular Immunology Division, The Walter and Eliza Hall Institute of Medical Research, Parkville, Victoria, Australia.*
[8]*Department of Medical Biology, The University of Melbourne, Parkville, Victoria, Australia.*
[9]*China-Australia Centre for Personalised Immunology, Dept of Rheumatology, Shanghai Renji Hospital, Shanghai JiaoTong University, Shanghai, China.*

Corresponding author: Carola G Vinuesa (carola.vinuesa@anu.edu.au).
Lead author: Jonathan Roco (jonathan.roco@anu.edu.au)

Summary

Class switch recombination (CSR) is a DNA recombination process that replaces the immunoglobulin (Ig) constant region for the isotype that can best protect against the pathogen. Dysregulation of CSR can cause self-reactive BCRs and B cell lymphomas; understanding the timing and location of CSR is therefore important. Although CSR commences upon T cell priming, it is generally considered a hallmark of germinal centers (GCs). Here we have used multiple approaches to show that CSR is triggered prior to differentiation into GC B cells or plasmablasts and is greatly diminished in GCs. Despite finding a small percentage of GC B cells expressing germline transcripts, phylogenetic trees of GC BCR from secondary lymphoid organs revealed that the vast majority of CSR events occurred prior to the onset of somatic hypermutation. As such, we have demonstrated the existence of IgM-dominated GCs, which are unlikely to occur under the assumption of ongoing switching.

Introduction

Class switch recombination (CSR) is an intrachromosomal DNA rearrangement of the immunoglobulin (Ig) heavy chain locus. As a result, IgM-IgD mature B cells are able to express antibodies of the IgA, IgG or IgE classes that differ in effector functions, without altering the specificity for the immunizing antigen (Stavnezer et al., 2008). CSR relies primarily on activation of the enzymes Activation-induced cytidine deaminase (AID), uracil-DNA glycosylase (UNG) and Apurinic-Apyrimidinic Endonuclease 1 (APE1) to specifically target intronic areas called switch (S) regions (Guikema et al., 2007; Muramatsu et al., 2000; Rada et al., 2002). DNA breaks introduced by these enzymes lead to the recombination of the variable heavy chain (VDJ) segment with a different constant heavy (C_H) chain gene (isotype) (Stavnezer et al., 2008). Selection of the appropriate isotype during infection is driven by cytokines and T cell help (Kawabe et al., 1994; Snapper and Mond, 1993), which induce transcription across the specific S regions with production of germline transcripts (GLTs) (Lorenz et al., 1995). GLTs (also known as switch-transcripts) are spliced, polyadenylated non-coding mRNAs transcribed from specific promoters located upstream of each set of S regions

(except for IgD). Expression of GLTs precedes DNA recombination of the Ig-C_H genes in B cells primed to undergo CSR (Stavnezer, 1996). For this reason, GLTs have long been used as a reliable molecular marker to study the onset of CSR *in vivo* (Cogné and Birshtein, 2004; Lorenz et al., 1995).

Germinal centers (GCs) are specialized microenvironments in secondary lymphoid organs, formed upon immunization. GCs are critical for the formation of long-lived plasma cells and memory B cells. Within these structures, B cells undergo somatic hypermutation (SHM) and clonal selection based on the affinity of the BCR for the immunizing antigen. Likewise, GCs are also considered to be the main areas where CSR takes place (Klein and Dalla-Favera, 2008; Vinuesa et al., 2009). Although SHM and CSR are two independent processes, both depend on the activity of AID (Muramatsu et al., 2000), which is expressed at highest amounts in GC B cells. These observations might have reinforced the idea that CSR is predominantly a GC process.

CSR has been predominantly studied using *in vitro* culture systems or after clonal expansion of B cells *in vivo*. In these studies, an important role of the GC environment in CSR has been postulated after finding GLTs are predominantly expressed by human cells bearing centrocyte-specific markers, including absence of CD77 (Liu et al., 1996). However these markers have been later shown to also identify activated B cells and plasmablasts (Hogerkorp and Borrebaeck, 2006). The association between CSR and GCs also comes from studies in genetically-manipulated mice with impaired formation of follicular structures that are likely to also perturb early T cell:B cell encounters (Shinkura et al., 1996). Nevertheless, extrafollicular (EF) responses are known to produce switched antibodies and induction of CSR has been detected as early as day 2 during a primary immune response (Cerutti, 2008; Fagarasan et al., 2001; Jacob et al., 1991; Pape et al., 2003; Toellner et al., 1996). Despite this evidence, it is still

generally believed that isotype-switching is an ongoing process that continues and is enhanced within GCs.

Here, we used transgenic mouse models that allow us to unequivocally distinguish GC B cells, extrafollicular plasmablasts (EFPBs) and their precursors from the earliest stages of an immune response *in vivo.* We show that CSR is initiated over the first few days in a primary response and prior to EF and GC commitment ceasing soon after B cells become GC cells and SHM commences. We also demonstrate the existence of IgM-dominated GCs which are unlikely to occur under the assumption of ongoing switching.

Results

GLT expression is triggered at the early stages of B cell activation and rapidly declines within GCs.

In order to identify the cells in which CSR is first triggered we took advantage of SW_{HEL} mice in which ~5-15% of the B cells carry a high-affinity BCR against hen egg lysozyme (HEL) (Phan et al., 2003). We adoptively transferred 3-15 x 10^4 SW_{HEL} B cells into C57BL/6 mice along with mutated HEL (HEL^{2x}) protein conjugated to sheep red blood cells (SRBCs) (Fig. 1A). SW_{HEL} B cells bind HEL^{2x} with moderate affinity and undergo CSR and SHM normally (Paus et al., 2006). Practically, all transferred B cells are known to be recruited into the response (Chan et al., 2009). As described in these previous studies, upon HEL-SRBC immunization adoptively-transferred SW_{HEL} B cells first appeared at the T cell:B cell border on day 1.5, at the periphery of the follicles on day 2.5, and within primary follicles on day 3 (Fig. 1B). On day 3.5, HEL-binding B cells were found forming nascent GCs and HEL-binding extrafollicular plasmablasts (EFPBs) were also seen (Fig. 1B). A homogeneous B cell population was observed by flow cytometry up to day 3 (Fig. 1C). Consistent with the immunofluorescence findings,

day 3.5 marked the appearance of GC B cells and EFPBs by flow cytometry. EFPBs were distinguished by downregulation of the chemokine receptor CXCR5 as well as B220 (Fig. 1C), shown to occur as B cells express BLIMP1 (Fig. 1D and S1A) and localize to extrafollicular foci (Chan et al., 2009). GC B cells seen at day 3.5 remained $CXCR5^{hi}$ $B220^{hi}$ (Fig. 1C) and also expressed FAS death receptor (Fig. S1A). These populations were sorted at 12h-24h intervals from day 1.5 after immunization and γ1 and γ2b-GLTs, the most abundant isotypes in the SRBC response (Phan et al., 2005), were quantified by qPCR. GLTs were first seen at day 1.5, peaked at day 2.5-3 prior to GC formation and declined rapidly thereafter to become barely detectable 48 hours later (Fig. 1E). Of note, total RNA amounts used for PCR amplification and RNA quality were comparable throughout the time-course (Fig. S2A). *Aicda* mRNA (encoding AID) was first detected at day 2.5; 12h after production of the first GLT and 24h prior to the appearance of EFPB or GC (Fig. 1E). Expression of *Bcl6*, the transcription factor required for GC B cell differentiation, was first detected at day 3.5 (Fig. 1E). Thus, CSR is triggered prior to EF or GC B cell commitment and GLTs decline prior to GC formation.

Class-switched antibodies are detected prior to GC formation and are comparable within GCs and EFPBs.

We next compared the production of surface IgG in GCs and EF foci (Fig. 2A-D). Class-switched B cells first appeared at day 2.5, one day after detection of the first GLT (Fig. 2B), coinciding with the earliest detection of *Aicda* mRNA (Fig. 1E). IgG^+ cells increased exponentially over the following two days, reaching a plateau from days 4.5 to 6.5 with approximately 70% of GC B cells and 90% of EFPBs having switched (Fig. 2C and 2D and Fig. S2B). The paucity of IgM^+ EFPBs at this time point may be due to the greater proliferative ability of switched cells (Martin and Goodnow, 2002; Tangye et al., 2003).

The affinity of SW_{HEL} B cells for HEL^{2x} is still quite high ($8x10^7$ M^{-1}) and there is some evidence that signal strength may play a role in driving early B cell events (Chan et al., 2009; Paus et al., 2006). To exclude the possibility that strong and uniform early-switching may have been driven by affinity; we repeated the experiments using HEL^{3x}, which carries an additional mutation that further lowers the affinity of the SW_{HEL} BCR interaction to 1.5 x 10^6 M^{-1} (Paus et al., 2006). We observed a small delay in the formation of GCs using HEL^{3x}; at day 3.5 HEL-binding B cells still appeared as a single population of activated B cells that haven't yet become GC cells (Fig. S3A). As seen with HEL^{2x}, γ1-GLT peaked at this pre-GC stage and a dramatic decline in GLTs was seen at the peak of the GC reaction (Fig. S3B-C). These results confirm that early and rapidly declining switching is a reproducible finding.

Germline transcription is rapidly induced at the T cell:B cell border

We next sought to visualize the precise location in which isotype-switching was initiated in C57BL/6 mice with a polyclonal BCR repertoire. For this we used Cγ1-Cre:mT/mG mice (Casola et al., 2006; Muzumdar et al., 2007), in which production of the γ1-GLT can be tracked by GFP expression. After SRBC immunization the first GFP^+ cells were detected on day 2 and were found predominantly at the T cell:B cell border (Fig. 2E). By day 3, GFP^+ cells had expanded and could be found within primary follicles that had yet not formed GCs. Within the following 48h GFP^+ cells were seen filling both GCs and extrafollicular foci. Thus, similar to the SW_{HEL} B cell response, class-switching is induced outside the follicles, 24h prior to GC formation.

Single cell profiling of DZ and LZ B cells reveals that germline transcripts are greatly diminished within GCs.

To ensure we were not underestimating GLT production in light zone (LZ) cells (centrocytes), thought to be the B cell subset in which germline transcription is activated (Liu et al., 1996), we performed single cell qPCR studies (Fig. 3A-E). Single

day 3 IgM^+ and day 6.5 IgM^+ SW_{HEL} GC B cells (Brink et al., 2015), subdivided into LZ and dark zone (DZ) cells according to CXCR4 and CD86 expression (Fig. 3A-B and Fig. S4A-B), were flow cytometry purified. Compared to 52% of day 3 activated B cells expressing γ1-GLT, less than 3% of DZ or LZ B cells expressed this transcript (Fig. 3C-E). Similar results were observed for γ2b-GLT, with 45% of day 3 B cells positive but only 4.8% and 1% of DZ and LZ B cells respectively expressing this GLT (Fig. 3C-E). Of note, 38% of GLT-positive B cells expressed more than one GLT.

It has been suggested that CSR requires Foxo1 and c-Myc transcription factor co-expression (Sander et al., 2015). Consistent with this, ~70% of day 3 B cells were Foxo1 and c-Myc double positive, and ~80% of these double positive cells expressed GLTs (Fig. S4C-D). By contrast, despite 41% of LZ cells expressing *Foxo1*, and 9% co-expressing *Foxo1* and c-*Myc* (Fig. S4C-D), none of the *Foxo1* and c-*Myc* double positive LZ cells expressed GLTs (Fig. S4D). This was also true for DZ B cells, with no double positive cells expressing GLTs (Fig. S4D). These results support the notion that GLT production leading to activation of CSR is not a feature of mature GCs.

Germline transcripts remain low in long-lived GCs.

We next sought to investigate responses to a different antigen and adjuvant and exclude the possibility that short-lived GCs such as those induced by SRBC may not be favorable to ongoing switching. For this, we transferred NP-reactive B1-8^{hi} $tdTomato^+$ (tdT^+) cells together with NP-CGG (Shih et al., 2002) into C57BL/6 mice primed with CGG in CFA 3 days earlier (Fig. 4A and Fig. S5A). This priming strategy makes the kinetics of the first few days comparable to that shown for SW_{HEL} responses (Fig. 1C), but with GCs persisting longer (Fig. 4B). Similar to the HEL^{2x}-SRBC response, γ1-GLT peaked between day 2-2.5 (Fig. 4C); at this time point, GLTs were found in cells with an intermediate phenotype ($CD38^{int}$ Fas^{int}) between EFPB and GC B cells (Fig. 4B-4C). GLTs had declined considerably by day 6.5 (Fig. 4C). At a later

stage of this immune response (day 14-18, Fig. 4D-4E), GC B cells maintained low amounts of γ1-GLT (Fig. 4F). Consistent with early induction of CSR, IgG expression in NP-binding B cells was first seen at day 2 (Fig. 4G). IgG^+ GC B cells peaked and reached a plateau between day 4 and day 8, remaining at constant numbers through day 18 (Fig. 4G), a period in which GCs were sustained (Fig. 4H). Thus, there was no evidence of reactivation or increased rates of Ig-switching in the late stages of the GC response.

The product of the episomes looped-out from the IgH locus after C_H gene recombination, known as switch circle transcripts, were assessed in all the adoptive transfer experiments performed. Despite efficient detection of switch circle transcripts in B cells activated *in vitro* (Fig. S5B-C), these byproducts of CSR could not be detected at any timepoint during the *in vivo* primary responses, either in pooled or single antigen-specific B cells (data not shown). This is likely to be due to the transient nature of these molecules and the low number of copies generated by a fraction of antigen-specific B cells. Of note, published studies measuring switch circle transcripts were conducted using *in vitro* culture systems or higher numbers of responding B cells such as those seen during reactivation of memory B cells (Kinoshita et al., 2001; Liu et al., 1996; McHeyzer-Williams et al., 2015; Wesemann et al., 2011).

Phylogenetic analysis reveals CSR occurs prior to the onset of SHM.

In order to assess CSR in mice with a polyclonal repertoire without the need for adoptive transfers that might lead to underestimation of ongoing switching, we determined the timing of CSR in polyclonal GCs through phylogenetic analysis (Fig. 5A-C). For this, we performed *in situ* photoactivation of single GCs within lymph nodes from GFP photoactivatable (GFP-PA) mice (Tas et al., 2016; Victora et al., 2010). This allows cells within the same GC to be fluorescently tagged, and then flow cytometry-sorted as single GC B cells. GFP-PA mice were immunized with CGG in alum, and

237 photoactivation followed by flow cytometry-purification performed 15 or 20 days later,
238 to allow multiple rounds of division and SHM within GCs. The SHM burden in the V-
239 region and the induction of recombination in the C_H region was assessed by *Igh* mRNA
240 sequencing in each cell. With this approach, clonal trees containing both switched and
241 unswitched B cells can be used to establish the timing of CSR, where the CSR point
242 can be inferred as the last common ancestor of the switched and unswitched cells.
243 Thus, the number of somatic mutations at the inferred CSR point serves as a
244 "molecular time stamp", which can be compared to the total SHM burden of cells
245 present in the GC at the time of analysis: CSR points occurring in cells with zero
246 mutations would indicate CSR precedes SHM and therefore occurs prior to GC onset;
247 whereas CSR points occurring in cells that have accumulated mutations would suggest
248 CSR is an ongoing process in GCs.
249
250 IgG1 is the most common isotype found in the CGG-alum response. To maximize the
251 possibility of identifying IgM to IgG1 CSR events, we screened GCs for expanded IgM^+
252 and IgG^+ B cell clones, including in the analysis clones containing ≥4 IgM^+ cells (Fig.
253 S6A). This approach led to sequencing 13 clones, including all 8 clones that contained
254 both IgM and IgG cells (Fig. 5A-B). Phylogenetic trees were displayed against the
255 number of somatic mutations in each cell (x-axis in Fig. 5B), where the inferred CSR
256 points are depicted as red filled triangles (Fig. 5B). We found that several trees
257 remained IgM, indicative of not having switched after entering the GC; these were
258 attributed a CSR point of zero (red open triangles, Fig. 5B). Whereas the overall
259 mutation burden in GC B cells was substantial (Fig. 5C, mean of 5 mutations per cell),
260 most clones had switch points at zero mutations, with a few at one mutation, and only
261 a single clone underwent switching at an inferred branch point bearing four mutations.
262 Importantly, we found a number of highly expanded and diversified clones (e.g, the top
263 two clones at days 15 and 20 in Fig. 5B) for which CSR was either not detected or
264 occurred in a common precursor with 0 or 1 mutations (Fig. 5B-C). Thus, substantial

SHM can occur in the absence of detectable CSR. Of note, no sequential switching events were detected in GCs, with IgG1, IgG2b and IgG3 always arising directly from IgM^+ cells (Fig. 5B). Similar findings were obtained from analysis of clonal trees within GCs from Peyer's patches: there were no CSR events within GC regardless of whether the trees were enriched in IgM^+, IgA^+ or $IgG2b^+$ cells (Fig. SX 5D-E). This data supports previous evidence that IgA switching predominantly occurs outside germinal centers (Reboldi et al., 2016). Mutational analysis of polyclonal GCs supports that CSR is restricted to the pre-GC or early GC periods, and is uncommon after cells have accumulated several mutations in mature GCs.

***In-silico* modelling of CSR predicts lack of ongoing switching in GCs.**

We found several IgM-dominated GCs (Fig. 5A, green-dominated columns). Prominent IgM^+ GC responses have been previously reported in responses to SRBC cells, although these are relatively short-lived (Shinall et al., 2000). Our detection of IgM-dominated GCs late in the response argues against ongoing switching. This prompted us to analyze *in silico* whether constant versus decaying CSR would differ in the distribution of isotype-dominated GCs (Binder and Meyer-Hermann, 2016; Meyer-Hermann, 2014; Meyer-Hermann et al., 2012). Analysis of the isotype diversity of *in silico* GCs revealed that with constant switching, the probability of finding IgM-dominated GCs was negligible (Fig. 5F), even when combined with a preferential output of switched GC B cells (Fig. 5G) (Martin and Goodnow, 2002). These results were generated with constant influx of IgM-dominated B cells until day 6 post immunization but still hold true with ongoing influx of IgM^+ B cells for longer time periods (Fig. S7A-B) or with a higher antigen-uptake rate of IgM B cells (Fig. S7C-D). Thus, given the observed mean IgG dominance of GCs at late time points, no tested isotype-specific differences allowed induction of both, IgM- and IgG-dominated GCs in the same setting, as required by our experimental results. In contrast, with a decaying switching probability using a decay constant derived from the dynamics of γ1-GLT

293 expression (Fig. 1E), a broad spectrum of IgM or IgG-dominated GCs develops (Fig.
294 5H). As we have seen IgM-dominated GCs (Fig. 5A-B), this result supports a model
295 with CSR limited to the first days of the GC reaction. Next, we shifted the time at which
296 the decay starts from day 3.5 post-immunization (GC onset) to day 19.5 in our *in silico*
297 model, keeping the integrated switching probability unchanged (Fig. 5I). The resulting
298 isotype diversity of GC simulations dropped when CSR occurred later than day 6-7
299 post-immunization (Fig. 5I). This suggests that a determination of the isotype before
300 the GC phase of intense B cell selection promotes diversification of the GC isotype
301 dominance at later times while an ongoing switching probability would homogenize the
302 isotype distribution of GC output.
303
304 **APE1 endonuclease is downregulated in germinal center B cells**
305 Our data so far demonstrated that downregulation of GLT production is a potent
306 mechanism to dampen CSR in GCs. We considered the possibility of additional
307 mechanisms that might contribute to limit CSR within GCs operating downstream of
308 GLT production. Once GLTs have been produced, CSR relies on activation of AID,
309 uracil-DNA glycosylase (UNG) and APE1 to target switch-regions (Guikema et al.,
310 2007; Muramatsu et al., 2000; Rada et al., 2002). APE1 is required in a dose-
311 dependent manner during CSR (Masani et al., 2013; Xu et al., 2014), whereas it is
312 dispensable for SHM (Stavnezer et al., 2014). By contrast, SHM does not need APE1
313 but instead requires APE2 (Masani et al., 2013; Sabouri et al., 2009; Stavnezer et al.,
314 2014). We compared RNA expression data of these enzymes in human naïve vs GC
315 B cells. Expression of *AID, UNG* and *APEX2* were all increased in GC B cells, whereas
316 *APEX1* appeared downregulated (Figure 6A). These observations are consistent with
317 a previous report in bulk mouse GC B cells (Stavnezer et al., 2014). We next asked
318 whether APE1 downregulation is a feature of both LZ and DZ B cells (Fig. 6B). Our
319 data revealed a significant decline in APE1 protein in both DZ and LZ areas of human
320 GCs (Fig. 6B-E). Thus, in addition to greatly diminished GLT induction in GC B cells,

APE1 downregulation emerges as an additional back up mechanism to prevent CSR in GCs.

BCL6 binds the promoter region of γ1-GLT and APE1

We next considered whether the BCL6 transcriptional repressor that determines GC B cell fate could contribute to the downregulation of GLTs, *Apex1* or both. BCL6 has been reported to bind to the ε-GLT promoter (Audzevich et al., 2013). We therefore tested whether this was also the case for the promoter of γ1-GLT. Bioinformatic analysis in the mouse promoter region of γ1-GLT revealed the presence of putative binding sites for BCL6 (Fig. S8A-C). We used ChIP-qPCR to validate this observation using the Nojima coculture system to induce *in vitro* derived GC (iGC) B cells (Nojima et al., 2011). We found that indeed, BCL6 binds the promoter region of γ1-GLT (Fig. S8D-E). Our analysis of published ChIP-on-chip data (Ci et al., 2009) revealed BCL6 was bound to the *APEX1*, but not *APEX2* promoter regions in human primary GC B cells (Fig. 6F) as well as to the promoters of the well-established BCL6 targets, *TLR1* and *BCL6*. Thus, BCL6 may also act as key regulator of CSR by actively repressing the transcription of GLTs and APE1 expression in GC B cells.

Discussion

Here we have shown that, unlike the prevailing idea that CSR is favored in GCs, this process largely occurs outside GCs. The association between CSR and GCs was first established when AID was discovered and shown to be expressed mainly in GCs, and essential for both SHM and CSR (Muramatsu et al., 2000). Further studies mapped the cells expressing GLTs in humans to centrocytes on the basis of markers no longer used (Liu et al., 1996) since they identify a heterogenous population that also contains activated B cells (Hogerkorp and Borrebaeck, 2006). Studies describing lack of CSR

in mice lacking GCs further cemented the notion that CSR was a GC process; these mice also had defective T cell:B cell encounters needed for CSR.

We have provided several lines of evidence that collectively show that isotype switching is activated before GC formation and rapidly declines as B cells differentiate in EFPBs or GCs during a primary immune response against TD-antigens. CSR, is initiated as early as day 1.5 following immunization and before GC formation via the production of GLTs. Analysis of GLT expression at the single cell level in purified IgM^+ activated B cells and IgM^+ GC B cells provided evidence that GLTs were produced at very small amounts in mature GCs. Phylogenetic trees constructed from Igh-mRNA sequencing of photoactivated GC B cells demonstrated that CSR ceased soon after the onset of SHM. These trees also revealed the existence of IgM-dominated GCs, which are unlikely to occur under the assumption of ongoing-switching. GLTs were first visualized at the T cell:B cell border prior to GC formation in a polyclonal B cell response using Cγ1-Cre:mT/mG mice and a comparable proportion of class-switched B cells were found in the EF and follicular areas of the spleen, with no further enrichment within GCs. This was independent of the immunizing antigen, the longevity of the GC response or the adjuvant used. Together, our work demonstrates early CSR with rapid decline in GCs, challenging the general belief that CSR is predominantly a GC process.

IgM^+ memory B cells are likely to be necessary to maintain a reservoir of antigen-experienced B cells (Reynaud et al., 2012) that can be rapidly engaged upon infection with either evolving or antigenically-related pathogens (Bernasconi et al., 2002; Pape et al., 2011) but are not functionally committed to any particular effector process, which includes preserving their capacity to switch to any isotype. This, in turn, would result in a much broader spectrum of antigen-specific B cells, both in terms of BCR affinities and functional properties, filling the memory B cell compartment after each

375 immunization. Our *in silico* modeling suggests that with constant CSR, the probability
376 of IgM^+ GC B cells, and by extrapolation antigen-experienced IgM^+ memory B cells, is
377 greatly diminished. By contrast, an early down-regulation of switching increases
378 isotype diversity. It is well known that humoral memory in humans can last for many
379 years, even decades. IgM^+ memory B cells are considered more stable over time
380 compared to their class-switched counterpart, and thus represent a reservoir of
381 lymphoid-memory that can be induced at recall when the titers of primary protective
382 antibodies have declined (Pape et al., 2011).
383
384 Lack of ongoing switching in GCs may be an important determinant of GC kinetics
385 given the evidence that IgM and IgG tails have different influences on B cell behavior
386 (Martin and Goodnow, 2002). It is possible that the larger GCs found in GCs of AID-
387 deficient mice that cannot undergo CSR and are therefore IgM-dominated (Muramatsu
388 et al., 2000) may reflect a greater permanence of IgM in GCs compared to their IgG
389 counterparts. There is some evidence that switched and unswitched memory B cells
390 have different transcriptional profiles (Seifert et al., 2015) suggesting important
391 functional differences. Understanding what these differences are will also help explain
392 further the biological significance of reducing CSR in GCs. It is likely that low
393 expression of AID, which is first detected on day 2.5, in conjunction with APE1 are
394 sufficient for CSR; whereas high expression of AID and APE2 in GCs might be required
395 for SHM. APE1 protein expression was reduced in GC B cells, including DZ and LZ B
396 cells. This data was confirmed by RNA-seq and in single cell studies, where fewer GC
397 B cells expressed *Apex1* mRNA compared to early-activated B cells. Whilst AID is
398 lowly expressed in recently activated B cells compared to GC B cells, CSR is
399 considered very efficient in nature (Stavnezer et al., 2008): AID can attack anywhere
400 within the S region, which can extend as long as 10-12kb, resulting in a high likelihood
401 of inducing the DNA breaks required for CSR. We therefore propose that CSR is
402 induced early during B cell activation, and then it is silenced in GCs due to several

mechanisms including a reduction in GLT production and a reduction in APE1 protein. The latter is likely mediated by the transcriptional repressor BCL6, as suggested by BCL6 binding to the *Apex1* promoter.

Our data is compatible with the notion that naïve B cells undergo CSR upon interacting with antigen and receiving T cell help prior to GC entry. We speculate that memory B cells may undergo CSR also upon interaction with T cells outside GCs, prior to differentiation into extrafollicular plasmablasts or re-entry into a GC. Sequential class-switching of memory B cells to downstream isotypes is well documented at least in the context of IgE responses (He et al., 2015). CSR not only appears to be repressed in GCs; previous studies have suggested that CSR also ceases upon B cell differentiation into plasmablasts in a BLIMP1-mediated manner (Shaffer et al., 2002). Lack of ongoing switching in GCs may be an important determinant of GC kinetics given the evidence that IgM and IgG tails have different influences on B cell behavior (Martin and Goodnow, 2002). It is possible that the larger GCs found in GCs of AID-deficient mice that cannot undergo CSR and are therefore IgM-dominated (Muramatsu et al., 2000) may reflect a greater permanence of IgM in GCs compared to their IgG counterparts.

Besides being the core apurinic-apyrimidinic endonuclease for CSR, APE1 is probably best known for its vital role in the BER-pathway, an important arm of the DNA damage response that repairs with high-fidelity damaged bases (Fortini and Dogliotti, 2007; Krokan and Bjoras, 2013). Under normal circumstances, APE1 recruits several BER components to execute the repair of AP-sites. Considering that APE1 is essential for cell survival and is ubiquitously expressed in all cells (Al-Safi et al., 2012; Fung and Demple, 2005; Xanthoudakis et al., 1996), the downregulation of APE1 in GC B cells is surprising, although in line with published data (Stavnezer et al., 2014). APE1 downregulation may explain how DNA lesions introduced during SHM are spared from correct repair by the error-free BER machinery (Stavnezer et al., 2014). Indeed, the

accurate repair of dU residues generated by AID and UNG would antagonize the acquisition of somatic mutations in the IgV region needed for correct affinity maturation. This idea is further supported by the findings that DNA Polβ is not downregulated in GC B cells (Schrader et al., 2009). Complete abrogation of the BER-pathway would be risky in cases where off-target mutations arising outside the Ig locus demand faithful repair.

Programmed DNA damage during SHM and CSR is a tightly regulated event, yet off-target activity of AID causing double-strand DNA breaks outside the IgV and S regions has also been reported and contributes to genomic instability (Liu and Schatz, 2009). Up to 95% of all lymphoid cancers are believed to have a B cell origin as a consequence of AID-dependent gene translocations and fusions or mutations affecting *cis*-regulatory elements (Nussenzweig and Nussenzweig, 2010). CSR itself is an important contributor to DNA lesions including aberrant gene translocations. Restricting CSR from taking place in GC B cells would help to reduce the likelihood of pathogenic double-strand breaks. Another potential advantage of limiting CSR in the GC comes from the observations of autoimmunity-inducing gene translocations or insertions occurring in the IgH locus during CSR (Nussenzweig and Nussenzweig, 2010; Tan et al., 2016): these occurrences would make this recombination process particularly risky in GCs, where not only cells are intensely proliferating, but also their output is destined to become long-lived memory B cells or plasma cells.

STAR Methods

Lead author: Jonathan Roco

Animals

C57BL/6, SW_{HEL} (Phan et al., 2003), B1-8^{hi} tdTomato (Shih et al., 2002), Cγ1Cre:mT/mG (Casola et al., 2006; Muzumdar et al., 2007), PA-GFP (Victora et al., 2010) and AID-Cre-Confetti (Tas et al., 2016) mice were bred and maintained in specific-pathogen-free conditions at the Australian National University (ANU), Canberra, Australia; The University of Birmingham, Birmingham UK; and The Rockefeller University, New York, USA. All experiments were performed according to the regulations approved by the local institution ethics committee, including the Australian National University's Animal and human Experimentation Ethics Committees.

Human samples

Human tonsils were obtained from consenting donors at The Canberra Hospital and Calvary John James Hospital (Canberra, ACT, Australia), following routine tonsillectomy. Tonsils were processed by mechanical disruption of the tissue and cells were isolated using Ficoll Hypaque (GE Healthcare Life Sciences) gradient centrifugation (Papa et al., 2017). All experiments with humans were approved by the Australian National University's Human Experimentation Ethics Committee and the University Hospitals Institutional Review Board.

SW_{HEL} B cell adoptive transfers

SW_{HEL} mice heterozygous for both light- and heavy-variable chain alleles of the anti-HEL BCR were sacrificed by cervical dislocation and splenocytes were collected. Single cell suspensions were obtained by mechanically disrupting the tissue through 70 µm nylon mesh filters (BD Bioscience) using complete RPMI 1640 media (Sigma-Aldrich). The exact frequency of SW_{HEL} B cells was determined by flow cytometry prior to adoptive transfer using HEL protein conjugated to Alexa Fluor 647 (A647). SW_{HEL} B cells ($CD45.1^+$) were resuspended in PBS1x and adoptively transferred (intravenous injection; *i.v.*) into congenic C57BL/6 recipient mice ($CD45.2^+$) along with $2x10^8$ sheep

red blood cells (SRBCs) conjugated to a mutated form of hen egg lysozyme (HEL^{2x}) (Paus et al., 2006). For experiments analyzing the early stages of the immune response (days 1.0 - 2.5) $1.5x10^5$ HEL-binding cells were transferred; whereas for analysis of late phases (days 3 - 8.5) $3x10^4$ cells were given.

B1-8^{hi} tdTomato (tdT) B cell adoptive transfers

C57BL/6 recipient mice (8-10 weeks old) were pre-immunized by intraperitoneal (*i.p.*) injection of 100 µg of chicken gamma globulin (CGG; #C-1000-10, Biosearch Techonolgies) emulsified in Complete Freund's adjuvant (CFA; #F5881, Sigma-Aldrich). Three days later, mice were intravenously transferred with B1-8^{hi} tdT$^+$ cells along with 50µg of 4-hydroxy-3-nitrophenyl acetyl (NP) conjugated to CGG (ratio 30-39, #N-5055D-5, Biosearch Technologies). This mixture was delivered in 200µL of PBS 1x. Single cell suspensions from B1-8^{hi} tdT$^+$ donor splenocytes were prepared in a similar fashion compared to SW_{HEL} B cell adoptive transfers. For investigation of early stages (17h - day 1.5) of the immune response $1.8x10^5$ B1-8^{hi} tdT$^+$ cells were transferred. For late stages (days 2 - 18) recipient mice received $6x10^4$ B1-8^{hi} tdT$^+$ cells. The exact frequency of B1-8^{hi} tdT cells was determined by flow cytometry prior to transfer, as measured by binding of the hapten NP conjugated to APC.

Flow cytometry analyses and FACS sorting

Single cells suspensions were prepared from mouse spleens, lymph nodes and human tonsils as previously described (Papa et al., 2017; Tas et al., 2016). After processing, cell subsets were examined using flow cytometry using the following antibodies. For mouse tissues: B220-APCCy7 (#103224, BioLegend), BLIMP1 (#150004, BioLegend), CD11b-A700 (#101222, BioLegend), CD11b-FITC (#553310, BD Bioscience), CD16/32 (mouse Fc-block, #553152, BD Bioscience), CD3-A700 (#100216, BioLegend), CD3-biotin (#100303, BioLegend), CD3-FITC (#553062, BD Bioscience), CD38-A700 (#56-0381-82, eBioscience), CD38-BV421 (#562768, BD Bioscience),

CD38-PE (#120707, BioLegend), CD45.1-PB (#110722, BioLegend), CD45.1-A700 (#110724, BioLegend), CD95-BV421 (#562633, BD Bioscience), CD95-PE (#554258, BD Bioscience), CXCR5-biotin (#551960, BD Bioscience), IgD-FITC (#11-5993-85, eBioscience), IgG1-biotin (#553441, BD Bioscience), IgG2a-biotin (#550332, BD Bioscience), IgG2b-biotin (#406704, BioLegend), IgG2c-biotin (#553504, BD Bioscience), IgG3-biotin (#553401, BD Bioscience), IgM-FITC (#553437, BD Bioscience), IgM-PECy7 (#25-5790-82, eBioscience), Streptavidin-APC (#S868, Thermo Fisher) and Streptavidin-BV605 (#405229, BioLegend). For human tonsils: CD19-PECy7 (#557835, BD Bioscience), CD27-FITC (#555440, BD Bioscience), CD38-PE (#347687, BD Bioscience), CD4-APCCy7 (#557871, BD Bioscience), CD86-A421 (#562432, BD Bioscience), CXCR4-APC (#306510, BioLegend) and Human TruStain FcX (Fc Receptor Blocking Solution, #422302, BioLegend). Antibody cocktails were prepared in flow cytometry buffer: PBS1x (Sigma-Aldrich) containing 2% fetal bovine serum (FBS, Gibco) and 2mM EDTA (Sigma-Aldrich). For detection of HEL-binding cells, HEL protein (Sigma-Aldrich) was conjugated to A647 using a protein labeling conjugation kit (Thermo Fisher). Dead cells were excluded using either 7-Aminoactinomycin D (7-AAD, Thermo Fisher) or Zombie aqua dye (#423102, BioLengend). Cells were stained with primary antibodies followed by secondary reagents for 30 min at 4°C in the dark. Intracellular stain was performed using the FOXP3 Transcription Factor Staining Buffer Set (#00552300, eBioscience) according to the manufacturer's instructions. Samples were acquired on a LSRII or Fortessa cytometer (BD) and analyzed using FlowJo software v10.3 (LLC).

Immunofluorescence

Frozen tissue sections were fixed in cold acetone for 10-20 min. Donor-derived SW_{HEL} B cells were detected in the spleen of recipient mice as previously described (Paus et al., 2006). T-cell areas were identified with anti-CD3-biotin antibody (#100303, BioLegend) followed by streptavidin conjugated to Alexa 350 (#S11249, Thermo Fisher). B cell follicles were visualized by staining with anti-IgD FITC (#11-5993-85, eBioscience). Cγ1-Cre:mT/mG spleen sections were stained with anti-CD3 (#550275, BD Pharmingen) and anti-IgD (#553438, BD Pharmingen) followed by biotin conjugated goat anti-hamster antibody (Jackson ImmunoResearch), streptavidin Alexa 405 (#S32351, Thermo Fisher) and donkey anti-rat Alexa-647 antibody (Jackson ImmunoResearch). For human samples, tonsil sections were blocked and permeabilized with 3% BSA (Sigma-Aldrich) and 0.5% Triton X-100 (Sigma-Aldrich). APE1 was detected using anti-APE1 antibody (sc-17774, Santa Cruz Biotechnology) followed by donkey anti-mouse Alexa 568 antibody (#A10037, Thermo Fisher). Follicles were identified using anti-human IgD-FITC antibody (#555778, BD Bioscience). Cell nuclei were counterstained using DAPI (Sigma-Aldrich). Stained sections were mounted using Vectashield (Vector Laboratories, #H-1200) and visualized using an Olympus IX71 inverted fluorescence microscope or a Zeiss Axio ScanZ1. Images were compiled using Photoshop CS6 software.

***In vitro* B cell cultures**

Flow cytometry purified human tonsil B cells were cultured in complete media: RPMI 1640 media (Sigma-Aldrich) supplemented with 2mM L-Glutamine (Gibco), 100 U penicillin-streptomycin (Gibco), 0.1mM nonessential amino acids (Gibco), 100mM Hepes (Gibco), 55mM β-mercaptoethanol (Gibco) and 10% FBS (Gibco). Cells were maintained for 72h in an incubator at 37°C with 5% CO_2.

Immunoblot

Naive, DZ and LZ B cells were isolated from human tonsils by flow cytometry. One fraction of naïve B cells was stimulated *in vitro* for 72h with IL-21 and CD40L (10ng/mL and 1µg/mL, respectively). Total protein extraction was performed using RIPA buffer (Thermo Fisher) supplemented with protease inhibitor (Roche). 10µg of whole-cell extracts from each cell subset were separated by SDS-PAGE (12% w/v), blotted onto nitro-cellulose membranes and incubated with anti-APE1 antibody (sc-17774, Santa Cruz Biotechnology). β-actin was used as a loading control (#A5441, Sigma-Aldrich). Enhanced chemiluminescence (ECL) development was performed after incubation with secondary antibodies conjugated to horseradish peroxidase (HRP) using Pierce ECL Western Blotting Substrate reagent (Thermo Fisher) according to manufacturer's instructions. Images were acquired on an Image Quant LAS 4000 machine (GE Healthcare Life Sciences). Densitometry analysis was performed using Image Studio software version 5.2.5 (LI-COR Biosciences).

qPCR analysis

Total RNA was extracted from mouse samples with Trizol (#15596026, Thermo Fisher). RNA quality and concentration were determined with an Agilent 2100 Bioanalyzer instrument. Only samples with a RIN score over 8 were selected for DNA digestion and cDNA synthesis using RQ1 RNase-Free DNase (#M6101, Promega) and SuperScript III Reverse Transcriptase (#18080093, Thermo Fisher), respectively. Duplex qPCR analyses were conducted for each target gene (FAM-labeled probe sets) using *Ubc* (VIC-labeled, Taqman assay #Mm01198158_m1, Thermo Fisher) or *Actb* (HEX-labeled probe set, Biosearch Technologies) as reference genes. Samples were measured in triplicate using an Applied Biosystems 7900HT Fast Real-Time machine (Thermo Fisher) with the following thermocycler condition: 50°C for 2 min (1 cycle); 95°C for 10 min (1 cycle); 40 cycles of 95°C for 15 sec and 60°C for 1min. For GLT-expression studies the following primers and dual-labeled BHQ probes were used:

γ1-GLT:

F: 5'-CGAGAAGCCTGAGGAATGTGT-3'

R: 5'-GGAGTTAGTTTGGGCAGCAGAT-3'

P: 5'-FAM-TGGTTCTCTCAACCTGTAGTCCATGCCA-3'

γ2b-GLT:

F: 5'-CGCACACCTACAGACAACCAG-3'

R: 5'-GTCACAGAGGAACCAGTTGTATC-3'

P: 5'-FAM-CCAGGGGGCCAGTGGATAGACTGAT-3'

γ2c-GLT:

F: 5'-GGACCACTAAAGCTGCTGACACAT-3'

R: 5'-AACCCTTGACCAGGCATCCT-3'

P: 5'-FAM-AGCCCCATCGGTCTATCCACTGGC-3'

γ3-GLT:

F: 5'-GACCAAATTCGCTGAGTCATCA-3'

R: 5'-ACCGAGGATCCAGATGTGTCA-3'

P: 5'-FAM-CTGTCTATCCCTTGGTCCCTGGCTGC-3'

μ-GLT:

F: 5'-TCTGGACCTCTCCGAAACCA-3'

R: 5'-ATGGCCACCAGATTCTTATCAGA-3'

P: 5'-FAM-ATGTCTTCCCCCTCGTCTCCTGCG-3'

Actb:

F: 5'-CGTGAAAAGATGACCCAGATCA-3'

R: 5'-TGGTACGACCAGAGGCATACAG-3'

P: 5'-HEX-TCAACACCCCAGCCATGTACGTAGCC-3'

These assays have been previously described (Marshall et al., 2011) and were manufactured by Biosearch Technologies. Data is expressed as a fold-change using the $\Delta\Delta C_T$ method.

One step qPCR analysis

Total RNA from 2,000-15,000 cells was purified using a PicoPure RNA Isolation Kit (#KIT0204, Thermo Fisher) according to the manufacturer's instructions. DNase treatment was performed on-column using RNase-Free DNase Set (#79254, Qiagen). Quality and concentration were determined as previously described using an Agilent 2100 Bioanalyzer instrument. Real-time one-step RT-PCR quantification was performed using the QuantiTect Multiplex RT-PCR Kit (#204643, Qiagen) in a final volume of 6µL. Duplex reactions with limiting primer concentrations were conducted in the same well for γ1-GLT (FAM-labeled probe set) and *Actb* (HEX-labeled probe set). Reactions were run in an Applied Biosystems 7900HT Fast Real-Time machine with the following thermocycler condition: 50°C for 20 min (1 cycle); 95°C for 15 min (1 cycle); 40 cycles of 94°C for 45 sec and 60°C for 45s. Expression of the target genes was normalized using the reference gene *Actb* and presented as a fold-change using the $\Delta\Delta C_T$ method.

Single cell qPCR

Single cell qPCR was performed as previously described (Nefzger et al., 2016). In brief, cells were flow cytometry deposited into qPCR 96-well plates filled with 10µL of lysis buffer and processed with the Single Cell to C_T kit (Life Technologies). cDNA was produced from the lysate as per kit's instructions. Samples were submitted to 18 cycles of pre-amplification using the following TaqMan assays (Thermo Fisher):

Actb (#Mm00607939_s1),

Foxo1 (#Mm00490672_m1),

Apex1 (#Mm01319526_g1),

Apex2 (#Mm00518685_m1),

Prdm1 (#Mm00476128_m1),

Bcl6 (#Mm00477633_m1),

Aicda (#Mm01184115_m1)

GLTs were detected using the probe sets previously described (see qPCR analysis section). Single cell qPCR data collection was performed with a Biomark instrument (Fluidigm) on pre-amplified templates that were positive screened for the housekeeper *Actb* (manually tested by qPCR). Reactions were run for 40 cycles. Data was analyzed using the Biomark software package "Real-Time PCR analysis" (Fluidigm). Data cleaning and normalization were done using custom R code (R version 3.3.3, R Core Team). The limit of detection was set to 40 cycles. Undetermined C_T were given a value of 40. Heatmaps and violin plots of the resulting data were generated using the ggplot2 package (version 2.2.1) in the R environment.

GC B cell clonal trees from photoactivatable (PA)-GFP-transgenic mice

PA-GFP-transgenic mice (Victora et al., 2010) were immunized with CGG-alum and draining popliteal lymph nodes (pLNs) were harvested 15 and 20 days later. Two individual GCs per pLN were photoactivated and single-cell sorted independently. Heavy-chain variable-segment (V_H) genes from individual B cells were amplified, sequenced and analyzed as described previously (Tas et al., 2016). Briefly, single cells were lysed in TCL buffer (Qiagen) with 1% β-mercaptoethanol. SPRI bead isolated RNA was reverse-transcribed into cDNA using an oligo(dT) primer. *Igh* and *Igk* transcripts were amplified from cDNA by PCR. Single-cell barcoded PCR amplicons were sequenced using the MiSeq platform (Illumina, MiSeq Reagent Nano Kit v2). Ig heavy variable (V), diversity (D) and joining (J) gene segments were assigned using the IMGT (Lefranc et al., 2009) and VBASE2 (Retter et al., 2005) databases. Functional V(D)J sequences were grouped into clones only when sharing *Ighv* and *Ighj* gene segments and junction regions (identical length and more than 75% amino acid identity in CDR3). Data for day 15 was re-analyzed from published sequences (Tas et al., 2016) using a similar methodology, and data for day 20 was generated *de novo* for this study. Only clones containing ≥ 3 IgM^+ cells, or at least one IgM^+ and one IgG^+ cell, were considered informative and are presented in this paper. Clonal phylogenies

and trees were constructed by the inference methodology algorithm GCtree (DeWitt et al., 2018).

Using AID-Cre-Confetti mice to track Peyer's Patch GCs

AID-Cre-Confetti mice (Tas et al., 2016) were used to visualize and track single GCs in the follicles of Peyer's Patches (PPs) of unimmunized mice. In these mice, upon the administration of tamoxifen, AID-expressing GC B cells are marked with one of ten fluorescent color combinations. In order to induced Cre-mediated recombination, 10 mg of tamoxifen in corn oil was administered twice by oral gavage two days apart. PP's were analyzed 18 days after the final administration of tamoxifen. Single PP's were isolated from the entire length of the small intestine and imaged with two-photon microscopy to locate single GC follicles. Individual GCs were then isolated by manual dissection prior to single-cell sorting. Following sorting, single cells were processed for sequencing as previously described.

Nojima cell co-cultures.

Co-cultures using the Nojima feeder cells were conducted as previously described (Nojima et al., 2011). Spleens were collected from C57BL/6 wild type mice and naïve B cells were magnetically purified using a B cell isolation kit (#130-090-862, Miltenyi Biotec) according to manufacture's instructions. The purified B cells were labelled with Cell Trace Violet (CTV) (#C34571, Thermo Fisher) according to manufacturer's instructions, and then co-cultured for 72h with Nojima feeder cells in complete media supplemented with recombinant murine IL-4 (10ng/μL, PeproTech). These *in vitro* derived GC (iGC) B cells were flow cytometry-purified to assess binding of Bcl6 to the γ1-GLT promoter by ChIP.

Chromatin immunoprecipitation (ChIP)-qPCR

ChIP-qPCR experiments were conducted as previously described (Kagey et al., 2010). Briefly, *in vitro* derived germinal centre B cells were flow cytometry-purified and then cross-linked with 1% formaldehyde for 10 min at room temperature, after which glycine was added to stop the reaction. Cells were washed three times with PBS 1x at 4°C, lysed with SDS-lysis buffer (1% SDS, 10mM EDTA, 50mM Tris-HCl pH 8) on ice for 10 min. Chromatin was sonicated using a Bioruptor instrument (Diagenode) to generate DNA fragments of 300-1000bp. Anti-Bcl6 (sc-858, Santa Cruz) antibody was used for ChIP. Amplification of ChIP DNA was performed using 2XSYBR Green PCR Master Mix (Applied Biosystems) in a 7900HT Fast Real-Time machine (Thermo Fisher). qPCR reactions were performed in duplicate with the following thermocycler condition: 50°C for 2 min (1 cycle); 95°C for 10 min (1 cycle); 40 cycles of 95°C for 15 sec and 60°C for 1 min. ChIP-qPCR data was normalized using the percent input method 2^(average C_T input – average C_T IP sample) (ThermoFisher). Primer sets used for ChIP-qPCR experiments are listed below:

Iγ1-P1:

F: 5'-GCTCCACCTACCTTGTCTTTAT-3'

R: 5'-GAGATGGGTTCAGAGTGTCATAG-3'

Iγ1-P2:

F: 5'-CACTCTCACTCCAGGGTATAGA-3'

R: 5'-TGAGACCCAGAACACAGAATTAG-3'

Iγ1-P3:

F: 5'-CTCCCACAACCTGTACCTAAAT-3'

R: 5'-GGACATGGAAGTAGAGGATCAAA-3'

Iγ1-P4:

F: 5'-GTCAGGAAAGAGTGGGCATAA-3'

R: 5'-CTGGCTGTACTCCTGTTTCTC-3'

Iγ1-TSS:

F: 5'-GGGCAGGACCAAAACAGGAA-3'

R: 5'-TTTCCCTGCTGACCCCACTC-3'

Bioinformatic analysis of ChIP-on-chip datasets and prediction of BCL6-binding sites in GLTs

Using ChIP-on-chip data (Ci et al., 2009) of BCL6 gene targets in human GC B cells, the APEX1 and APEX2 loci were analyzed for BCL6 binding peaks as previously described (Ci et al., 2009). The known BCL6 targets *TLR1* and *BCL6* were used as controls. The data set was obtained from GEO, accession number GSE15179. BCL6 binding sites in the γ1-GLT promoter were predicted using the JASPAR 2018 database (Khan et al., 2018).

Statistical Analysis

Datasets were analyzed using Mann-Whitney test (U test, two-tailed), except for quantification of western blots, in which a paired t-test (two-tailed) was used. To compare more than two groups or sets of data a Kruskal-Wallis test was performed followed by Dunn's post-test. The test employed to analyze the different experiments is indicated in each figure legend. Statistical tests were selected based on the distribution and the variance characteristics of the data. Normality was assessed with Shapiro-Wilk test. All statistical analyzes were performed with Prism software version 7 (GraphPad Software) and R software version 3.3.3 (R Core Team). The exact *p*-values are shown in each figure.

Mathematical modeling

All simulations are based on a previously published agent-based model of B and T cell dynamics within the GC (Meyer-Hermann et al., 2012), which lacks an isotype switching model (see below). Briefly, the model describes dynamics of B and T cells in discrete three-dimensional space including diffusion of chemotactic signals that

754 influence cell motility. The GC reaction starts with founder B cells migrating into the
755 virtual GC area within the first four days at a rate of 2 cells per hour (of note, the B cell
756 influx was prolonged in supplementary Fig. S7A). Each B cell divides six times before
757 it is allowed to differentiate to a LZ phenotype that depends on antigen collection for
758 survival beyond a critical time period. Antigen is collected by B cells in an affinity-
759 dependent manner, where affinity of a B cell for an antigen is represented by Hamming
760 distance in four-dimensional shape space. Furthermore, B cells depend on T cell help
761 for survival. For competing B cells, T follicular helper (T_{FH}) cells polarize towards the
762 cell with the higher amounts of collected and processed antigen. B cells collect T_{FH}
763 signals and require a sufficient total amount of collected signal for survival. Each
764 selected B cell returns to the DZ and divides a number of times that depends on the
765 amount of collected antigen, a mechanism termed dynamic number of divisions
766 (Meyer-Hermann, 2014) and supported by experimental data (Gitlin et al., 2014).
767 Differentiation to GC output cells is induced in a probabilistic manner (LEDAX model)
768 (Meyer-Hermann et al., 2012). A full description of the modeling framework and its
769 compatibility with recent experimental data has been recently published (Binder and
770 Meyer-Hermann, 2016).
771
772 For the present context of B cell isotype switching, a new model of GC dynamics
773 needed to be developed, which explicitly represents the different isotypes and allows
774 for different models of how isotype switching happens. Newly arrived cells are
775 assumed to predominantly express IgM. In accordance with early measurements of
776 the amount of IgG^+ B cells (Fig. 1C and Fig. 2A-D), we assume that 35% of the founder
777 cells are already expressing IgG. At each division event, the daughter cells switch from
778 IgM to IgG with a defined probability. This switching probability *p* can be either constant
779 or decrease over time according to an exponential decay model with a half-life
780 corresponding to the observed decrease in GLTs (Fig. 1E), $p(t) = p_0\, e^{-\gamma t}$, where p_0
781 denotes the switching probability at the beginning and γ is the decay of the switching

probability over time. The initial switching probability is not a free parameter, this was determined by data on the relative amount of either isotype at later time points of the reaction in Fig. 4F and 4G for both the constant (p = 0.03 at each division, unless stated otherwise) and the dynamic (p_0 = 0.15 at each division) switching model separately.

To account for a possible preferential output for the IgG isotype, we introduced a bias factor, η, that increases the probability for IgG^+ cells to become plasma cells while decreasing the output probability for IgM^+ cells by the same amount, keeping the total amount of output cells comparable. The different conditions were simulated in 400 *in silico* GCs and the distribution of the fraction of IgG^+ B cells at day 21 after onset of the GC reaction was evaluated among these 400 GCs.

To test for the impact of the timing of CSR, we combined the dynamic switching model with a delay in switching, leading to a limited time interval for switching at different times of the GC reaction. We tested a delay of different time intervals, t_{switch} (Fig. 5G). Each delay was simulated in 400 GCs and the diversity of the IgG fraction at day 21 within these 400 simulations was assessed using the difference between the upper and the lower quartile (interquartile range, IQR).

All simulations were performed using custom C++ code. Simulation output was analyzed using the R statistics language; plots of the simulation output were created using the ggplot2 library.

References

Al-Safi, R.I., Odde, S., Shabaik, Y., and Neamati, N. (2012). Small-molecule inhibitors of APE1 DNA repair function: an overview. Curr Mol Pharmacol *5*, 14-35.

Audzevich, T., Pearce, G., Breucha, M., Gunal, G., and Jessberger, R. (2013). Control of the STAT6-BCL6 antagonism by SWAP-70 determines IgE production. J Immunol *190*, 4946-4955.

Bernasconi, N.L., Traggiai, E., and Lanzavecchia, A. (2002). Maintenance of serological memory by polyclonal activation of human memory B cells. Science *298*, 2199-2202.

Binder, S.C., and Meyer-Hermann, M. (2016). Implications of Intravital Imaging of Murine Germinal Centers on the Control of B Cell Selection and Division. Front Immunol *7*, 593.

Brink, R., Paus, D., Bourne, K., Hermes, J.R., Gardam, S., Phan, T.G., and Chan, T.D. (2015). The SW(HEL) system for high-resolution analysis of in vivo antigen-specific T-dependent B cell responses. Methods Mol Biol *1291*, 103-123.

Casola, S., Cattoretti, G., Uyttersprot, N., Koralov, S.B., Seagal, J., Hao, Z., Waisman, A., Egert, A., Ghitza, D., and Rajewsky, K. (2006). Tracking germinal center B cells expressing germ-line immunoglobulin gamma1 transcripts by conditional gene targeting. Proc Natl Acad Sci U S A *103*, 7396-7401.

Cerutti, A. (2008). The regulation of IgA class switching. Nat Rev Immunol *8*, 421-434.

Chan, T.D., Gatto, D., Wood, K., Camidge, T., Basten, A., and Brink, R. (2009). Antigen affinity controls rapid T-dependent antibody production by driving the expansion rather than the differentiation or extrafollicular migration of early plasmablasts. J Immunol *183*, 3139-3149.

Ci, W., Polo, J.M., Cerchietti, L., Shaknovich, R., Wang, L., Yang, S.N., Ye, K., Farinha, P., Horsman, D.E., Gascoyne, R.D.*, et al.* (2009). The BCL6 transcriptional program features repression of multiple oncogenes in primary B cells and is deregulated in DLBCL. Blood *113*, 5536-5548.

Cogné, M., and Birshtein, B.K. (2004). CHAPTER 19 - Regulation of Class Switch Recombination A2 - Honjo, Tasuku. In Molecular Biology of B Cells, F.W. Alt, and M.S. Neuberger, eds. (Burlington: Academic Press), pp. 289-305.

DeWitt, W.S., 3rd, Mesin, L., Victora, G.D., Minin, V.N., and Matsen, F.A.t. (2018). Using Genotype Abundance to Improve Phylogenetic Inference. Mol Biol Evol *35*, 1253-1265.

Di Noia, J.M., and Neuberger, M.S. (2007). Molecular mechanisms of antibody somatic hypermutation. Annu Rev Biochem *76*, 1-22.

Fagarasan, S., Kinoshita, K., Muramatsu, M., Ikuta, K., and Honjo, T. (2001). In situ class switching and differentiation to IgA-producing cells in the gut lamina propria. Nature *413*, 639-643.

Fortini, P., and Dogliotti, E. (2007). Base damage and single-strand break repair: mechanisms and functional significance of short- and long-patch repair subpathways. DNA Repair (Amst) *6*, 398-409.

Fung, H., and Demple, B. (2005). A vital role for Ape1/Ref1 protein in repairing spontaneous DNA damage in human cells. Mol Cell *17*, 463-470.

Gazumyan, A., Bothmer, A., Klein, I.A., Nussenzweig, M.C., and McBride, K.M. (2012). Activation-induced cytidine deaminase in antibody diversification and chromosome translocation. Adv Cancer Res *113*, 167-190.

Gitlin, A.D., Shulman, Z., and Nussenzweig, M.C. (2014). Clonal selection in the germinal centre by regulated proliferation and hypermutation. Nature *509*, 637-640.

Guikema, J.E., Linehan, E.K., Tsuchimoto, D., Nakabeppu, Y., Strauss, P.R., Stavnezer, J., and Schrader, C.E. (2007). APE1- and APE2-dependent DNA breaks in immunoglobulin class switch recombination. J Exp Med *204*, 3017-3026.

He, J.S., Narayanan, S., Subramaniam, S., Ho, W.Q., Lafaille, J.J., and Curotto de Lafaille, M.A. (2015). Biology of IgE production: IgE cell differentiation and the memory of IgE responses. Curr Top Microbiol Immunol *388*, 1-19.

Hogerkorp, C.M., and Borrebaeck, C.A. (2006). The human CD77- B cell population represents a heterogeneous subset of cells comprising centroblasts, centrocytes, and plasmablasts, prompting phenotypical revision. J Immunol *177*, 4341-4349.

Jacob, J., Kassir, R., and Kelsoe, G. (1991). In situ studies of the primary immune response to (4-hydroxy-3-nitrophenyl)acetyl. I. The architecture and dynamics of responding cell populations. J Exp Med *173*, 1165-1175.

Kagey, M.H., Newman, J.J., Bilodeau, S., Zhan, Y., Orlando, D.A., van Berkum, N.L., Ebmeier, C.C., Goossens, J., Rahl, P.B., Levine, S.S.*, et al.* (2010). Mediator and cohesin connect gene expression and chromatin architecture. Nature *467*, 430-435.

Kawabe, T., Naka, T., Yoshida, K., Tanaka, T., Fujiwara, H., Suematsu, S., Yoshida, N., Kishimoto, T., and Kikutani, H. (1994). The immune responses in CD40-deficient mice: impaired immunoglobulin class switching and germinal center formation. Immunity *1*, 167-178.

Khan, A., Fornes, O., Stigliani, A., Gheorghe, M., Castro-Mondragon, J.A., van der Lee, R., Bessy, A., Cheneby, J., Kulkarni, S.R., Tan, G.*, et al.* (2018). JASPAR 2018: update of the open-access database of transcription factor binding profiles and its web framework. Nucleic Acids Res *46*, D1284.

Kinoshita, K., Harigai, M., Fagarasan, S., Muramatsu, M., and Honjo, T. (2001). A hallmark of active class switch recombination: transcripts directed by I promoters on looped-out circular DNAs. Proc Natl Acad Sci U S A *98*, 12620-12623.

Klein, U., and Dalla-Favera, R. (2008). Germinal centres: role in B-cell physiology and malignancy. Nat Rev Immunol *8*, 22-33.

Krokan, H.E., and Bjoras, M. (2013). Base excision repair. Cold Spring Harb Perspect Biol *5*, a012583.

885 Lefranc, M.P., Giudicelli, V., Ginestoux, C., Jabado-Michaloud, J., Folch, G.,
886 Bellahcene, F., Wu, Y., Gemrot, E., Brochet, X., Lane, J.*, et al.* (2009). IMGT, the
887 international ImMunoGeneTics information system. Nucleic Acids Res *37*, D1006-
888 1012.

889 Liu, M., and Schatz, D.G. (2009). Balancing AID and DNA repair during somatic
890 hypermutation. Trends Immunol *30*, 173-181.

891 Liu, Y.J., Malisan, F., de Bouteiller, O., Guret, C., Lebecque, S., Banchereau, J., Mills,
892 F.C., Max, E.E., and Martinez-Valdez, H. (1996). Within germinal centers, isotype
893 switching of immunoglobulin genes occurs after the onset of somatic mutation.
894 Immunity *4*, 241-250.

895 Lorenz, M., Jung, S., and Radbruch, A. (1995). Switch transcripts in immunoglobulin
896 class switching. Science *267*, 1825-1828.

897 Marshall, J.L., Zhang, Y., Pallan, L., Hsu, M.C., Khan, M., Cunningham, A.F.,
898 MacLennan, I.C., and Toellner, K.M. (2011). Early B blasts acquire a capacity for Ig
899 class switch recombination that is lost as they become plasmablasts. Eur J Immunol
900 *41*, 3506-3512.

901 Martin, S.W., and Goodnow, C.C. (2002). Burst-enhancing role of the IgG membrane
902 tail as a molecular determinant of memory. Nat Immunol *3*, 182-188.

903 Masani, S., Han, L., and Yu, K. (2013). Apurinic/apyrimidinic endonuclease 1 is the
904 essential nuclease during immunoglobulin class switch recombination. Mol Cell Biol
905 *33*, 1468-1473.

906 McHeyzer-Williams, L.J., Milpied, P.J., Okitsu, S.L., and McHeyzer-Williams, M.G.
907 (2015). Class-switched memory B cells remodel BCRs within secondary germinal
908 centers. Nat Immunol *16*, 296-305.

909 Meyer-Hermann, M. (2014). Overcoming the dichotomy of quantity and quality in
910 antibody responses. J Immunol *193*, 5414-5419.

911 Meyer-Hermann, M., Mohr, E., Pelletier, N., Zhang, Y., Victora, G.D., and Toellner,
912 K.M. (2012). A theory of germinal center B cell selection, division, and exit. Cell Rep
913 *2*, 162-174.

914 Muramatsu, M., Kinoshita, K., Fagarasan, S., Yamada, S., Shinkai, Y., and Honjo, T.
915 (2000). Class switch recombination and hypermutation require activation-induced
916 cytidine deaminase (AID), a potential RNA editing enzyme. Cell *102*, 553-563.

917 Muzumdar, M.D., Tasic, B., Miyamichi, K., Li, L., and Luo, L. (2007). A global double-
918 fluorescent Cre reporter mouse. Genesis *45*, 593-605.

919 Nefzger, C.M., Jarde, T., Rossello, F.J., Horvay, K., Knaupp, A.S., Powell, D.R., Chen,
920 J., Abud, H.E., and Polo, J.M. (2016). A Versatile Strategy for Isolating a Highly
921 Enriched Population of Intestinal Stem Cells. Stem Cell Reports *6*, 321-329.

922 Nojima, T., Haniuda, K., Moutai, T., Matsudaira, M., Mizokawa, S., Shiratori, I., Azuma,
923 T., and Kitamura, D. (2011). In-vitro derived germinal centre B cells differentially
924 generate memory B or plasma cells in vivo. Nat Commun *2*, 465.

925 Nussenzweig, A., and Nussenzweig, M.C. (2010). Origin of chromosomal
926 translocations in lymphoid cancer. Cell *141*, 27-38.

927 Papa, I., Saliba, D., Ponzoni, M., Bustamante, S., Canete, P.F., Gonzalez-Figueroa,
928 P., McNamara, H.A., Valvo, S., Grimbaldeston, M., Sweet, R.A*., et al.* (2017). TFH-
929 derived dopamine accelerates productive synapses in germinal centres. Nature *547*,
930 318-323.

931 Pape, K.A., Kouskoff, V., Nemazee, D., Tang, H.L., Cyster, J.G., Tze, L.E., Hippen,
932 K.L., Behrens, T.W., and Jenkins, M.K. (2003). Visualization of the genesis and fate of
933 isotype-switched B cells during a primary immune response. J Exp Med *197*, 1677-
934 1687.

935 Pape, K.A., Taylor, J.J., Maul, R.W., Gearhart, P.J., and Jenkins, M.K. (2011). Different
936 B cell populations mediate early and late memory during an endogenous immune
937 response. Science *331*, 1203-1207.

938 Paus, D., Phan, T.G., Chan, T.D., Gardam, S., Basten, A., and Brink, R. (2006).
939 Antigen recognition strength regulates the choice between extrafollicular plasma cell
940 and germinal center B cell differentiation. J Exp Med *203*, 1081-1091.

941 Phan, T.G., Amesbury, M., Gardam, S., Crosbie, J., Hasbold, J., Hodgkin, P.D.,
942 Basten, A., and Brink, R. (2003). B cell receptor-independent stimuli trigger
943 immunoglobulin (Ig) class switch recombination and production of IgG autoantibodies
944 by anergic self-reactive B cells. J Exp Med *197*, 845-860.

945 Phan, T.G., Gardam, S., Basten, A., and Brink, R. (2005). Altered migration,
946 recruitment, and somatic hypermutation in the early response of marginal zone B cells
947 to T cell-dependent antigen. J Immunol *174*, 4567-4578.

948 Rada, C., Williams, G.T., Nilsen, H., Barnes, D.E., Lindahl, T., and Neuberger, M.S.
949 (2002). Immunoglobulin isotype switching is inhibited and somatic hypermutation
950 perturbed in UNG-deficient mice. Curr Biol *12*, 1748-1755.

951 Reboldi, A., Arnon, T.I., Rodda, L.B., Atakilit, A., Sheppard, D., and Cyster, J.G. (2016).
952 IgA production requires B cell interaction with subepithelial dendritic cells in Peyer's
953 patches. Science *352*, aaf4822.

954 Retter, I., Althaus, H.H., Munch, R., and Muller, W. (2005). VBASE2, an integrative V
955 gene database. Nucleic Acids Res *33*, D671-674.

956 Reynaud, C.A., Descatoire, M., Dogan, I., Huetz, F., Weller, S., and Weill, J.C. (2012).
957 IgM memory B cells: a mouse/human paradox. Cell Mol Life Sci *69*, 1625-1634.

958 Sabouri, Z., Okazaki, I.M., Shinkura, R., Begum, N., Nagaoka, H., Tsuchimoto, D.,
959 Nakabeppu, Y., and Honjo, T. (2009). Apex2 is required for efficient somatic
960 hypermutation but not for class switch recombination of immunoglobulin genes. Int
961 Immunol *21*, 947-955.

962 Sander, S., Chu, V.T., Yasuda, T., Franklin, A., Graf, R., Calado, D.P., Li, S., Imami,
963 K., Selbach, M., Di Virgilio, M*., et al.* (2015). PI3 Kinase and FOXO1 Transcription
964 Factor Activity Differentially Control B Cells in the Germinal Center Light and Dark
965 Zones. Immunity *43*, 1075-1086.

966 Schrader, C.E., Guikema, J.E., Wu, X., and Stavnezer, J. (2009). The roles of APE1,
967 APE2, DNA polymerase beta and mismatch repair in creating S region DNA breaks
968 during antibody class switch. Philos Trans R Soc Lond B Biol Sci *364*, 645-652.

969 Seifert, M., Przekopowitz, M., Taudien, S., Lollies, A., Ronge, V., Drees, B.,
970 Lindemann, M., Hillen, U., Engler, H., Singer, B.B.*, et al.* (2015). Functional capacities
971 of human IgM memory B cells in early inflammatory responses and secondary germinal
972 center reactions. Proc Natl Acad Sci U S A *112*, E546-555.

973 Shaffer, A.L., Lin, K.I., Kuo, T.C., Yu, X., Hurt, E.M., Rosenwald, A., Giltnane, J.M.,
974 Yang, L., Zhao, H., Calame, K.*, et al.* (2002). Blimp-1 orchestrates plasma cell
975 differentiation by extinguishing the mature B cell gene expression program. Immunity
976 *17*, 51-62.

977 Shih, T.A., Roederer, M., and Nussenzweig, M.C. (2002). Role of antigen receptor
978 affinity in T cell-independent antibody responses in vivo. Nat Immunol *3*, 399-406.

979 Shinall, S.M., Gonzalez-Fernandez, M., Noelle, R.J., and Waldschmidt, T.J. (2000).
980 Identification of murine germinal center B cell subsets defined by the expression of
981 surface isotypes and differentiation antigens. J Immunol *164*, 5729-5738.

982 Shinkura, R., Matsuda, F., Sakiyama, T., Tsubata, T., Hiai, H., Paumen, M., Miyawaki,
983 S., and Honjo, T. (1996). Defects of somatic hypermutation and class switching in
984 alymphoplasia (aly) mutant mice. Int Immunol *8*, 1067-1075.

985 Snapper, C.M., and Mond, J.J. (1993). Towards a comprehensive view of
986 immunoglobulin class switching. Immunol Today *14*, 15-17.

987 Stavnezer, J., Guikema, J.E., and Schrader, C.E. (2008). Mechanism and regulation
988 of class switch recombination. Annu Rev Immunol *26*, 261-292.

989 Stavnezer, J., Linehan, E.K., Thompson, M.R., Habboub, G., Ucher, A.J., Kadungure,
990 T., Tsuchimoto, D., Nakabeppu, Y., and Schrader, C.E. (2014). Differential expression
991 of APE1 and APE2 in germinal centers promotes error-prone repair and A:T mutations
992 during somatic hypermutation. Proc Natl Acad Sci U S A *111*, 9217-9222.

993 Tan, J., Pieper, K., Piccoli, L., Abdi, A., Foglierini, M., Geiger, R., Tully, C.M.,
994 Jarrossay, D., Ndungu, F.M., Wambua, J.*, et al.* (2016). A LAIR1 insertion generates
995 broadly reactive antibodies against malaria variant antigens. Nature *529*, 105-109.

996 Tangye, S.G., Avery, D.T., Deenick, E.K., and Hodgkin, P.D. (2003). Intrinsic
997 differences in the proliferation of naive and memory human B cells as a mechanism
998 for enhanced secondary immune responses. J Immunol *170*, 686-694.

999 Tas, J.M., Mesin, L., Pasqual, G., Targ, S., Jacobsen, J.T., Mano, Y.M., Chen, C.S.,
1000 Weill, J.C., Reynaud, C.A., Browne, E.P.*, et al.* (2016). Visualizing antibody affinity
1001 maturation in germinal centers. Science *351*, 1048-1054.

1002 Toellner, K.M., Gulbranson-Judge, A., Taylor, D.R., Sze, D.M., and MacLennan, I.C.
1003 (1996). Immunoglobulin switch transcript production in vivo related to the site and time
1004 of antigen-specific B cell activation. J Exp Med *183*, 2303-2312.

1005 Victora, G.D., Schwickert, T.A., Fooksman, D.R., Kamphorst, A.O., Meyer-Hermann,
1006 M., Dustin, M.L., and Nussenzweig, M.C. (2010). Germinal center dynamics revealed

by multiphoton microscopy with a photoactivatable fluorescent reporter. Cell *143*, 592-605.

Vinuesa, C.G., Sanz, I., and Cook, M.C. (2009). Dysregulation of germinal centres in autoimmune disease. Nat Rev Immunol *9*, 845-857.

Wesemann, D.R., Magee, J.M., Boboila, C., Calado, D.P., Gallagher, M.P., Portuguese, A.J., Manis, J.P., Zhou, X., Recher, M., Rajewsky, K.*, et al.* (2011). Immature B cells preferentially switch to IgE with increased direct Smu to Sepsilon recombination. J Exp Med *208*, 2733-2746.

Xanthoudakis, S., Smeyne, R.J., Wallace, J.D., and Curran, T. (1996). The redox/DNA repair protein, Ref-1, is essential for early embryonic development in mice. Proc Natl Acad Sci U S A *93*, 8919-8923.

Xu, J., Husain, A., Hu, W., Honjo, T., and Kobayashi, M. (2014). APE1 is dispensable for S-region cleavage but required for its repair in class switch recombination. Proc Natl Acad Sci U S A *111*, 17242-17247.

Acknowledgments

C.G.V. is supported by fellowship, project, and program grants from the Australian National Health and Medical Research Council. The Human Frontier Science Program (RGP0033/2015) supports M.M.H., G.V. and C.G.V.

Author contributions statement

J.R. conducted most of the experiments, figure editing and data analysis. P.G., P.C., J.E., Q.S. and J.C. helped with the experiments, human sample processing and provided intellectual input. H.V. provided intellectual input and expertise in the analysis and acquisition of flow cytometry data. L.M.C provided help with the analysis of RNA-seq data. K.M.T. provided intellectual input, helped in the design of single cell studies and together with Y.Z. performed the Cγ1-Cre:mT/mG mouse experiments. L.M., C.N., A.S. and G.V. performed the experiments using the PA-GFP and the AID-Cre-Confetti mouse models, generation of clonal trees, provided intellectual input and contributed to data analysis. S.C.B., P.R. and M.M.H. provided intellectual input and performed the *in silico* modeling. C.N., J.R. and J.P. conducted the single cell qPCR studies. J.R. and C.G.V. wrote the manuscript. C.G.V. was the main supervisor of this project. All authors reviewed the manuscript.

Competing interests

The authors declare no competing financial interests.

Data and materials availability

Data and materials can be made available upon request to the corresponding author.

Code availability

Custom code used in this study can be made available upon request to the corresponding author.

Legends to Figures

Figure 1. Isotype switching commences prior to germinal center onset.

A) Adoptive transfer protocol of SW_{HEL} B cells and HEL^{2x}-SRBCs into congenic recipient mice (see STAR Methods).

B) Immunofluorescence images of spleen sections collected from recipient mice as in **(A)**. Sections were stained for SW_{HEL} B cells (red), IgD (green), and CD3 (blue). Scale bars = 200 μm.

C-D) Representative flow cytometric plots showing gating strategy to identified donor-derived Sw_{HEL} B cells after adoptive transfer **(C)** and expression (**D**) of BLIMP1 vs CXCR5 or B220, and Fas vs CXCR5 in HEL-binding B cells recovered 5 days after challenge as shown in **(A)**.

E) qPCR gene expression profile of purified donor-derived SW_{HEL} B cells for γ1-GLT, γ2b-GLT, *Aicda, and Bcl6*. Data was normalized to the reference gene *Ubc* and is presented as a fold-change compared to day 3.5 values using the $\Delta\Delta C_T$ method. Dots represent the mean of pooled biological replicates as in **(C)**.

Data is representative of two independent experiments. n = number of recipient mice used at each time point. Please also see Figure SX.

Figure 2. Class switching proceeds at comparable rates in germinal centers and extrafollicular sites and early visualization of germline transcription in a polyclonal response.

A) Flow cytometric plots showing gating strategy employed to identify donor-derived SW_{HEL} B cells after immunization as shown in Figure 1.

B-C) Flow cytometric analysis for surface expression of IgG1 and IgM in naïve (day 0), activated (day 2.5) **(B)**, EFPB and GC SW_{HEL} B cells (day 4.5 - 6.5) **(C)**. Numbers indicate the percentage of donor-derived HEL^+ $IgG1^+$ cells.

D) Quantification of IgG1, IgG2b and total IgG in EFPBs or GC B cells as shown in **(C)**. Bars represent medians and dots individual mice (n=4). Horizontal grey bars show comparisons between EFPB and GC subsets at the same time point (Mann-Whitney U test). Horizontal purple and blue bars show comparisons between EFPBs or GC B cells (Kruskal-Wallis test), respectively. Numbers on top of bars indicate the respective *p*-value. ns = not significant.

E) Immunofluorescence images of spleen sections from Cγ1-Cre:mT/mG mice after SRBC immunization at the indicated time points: CD3 (grey), IgD (blue), Cγ1-Cre (green) and non-activated B cells (red).

Data is representative of two (A-D) and three (E) independent experiments. Please also see Figure SX.

Figure 3. Single cell analysis of germline transcripts in early activated and GC B cells.

A-B) Flow cytometry plots showing gating strategy to purify HEL-binding B cells after HEL^{2x}-SRBC immunization. Donor-derived cells were single cell purified as $IgM^{+}HEL^{+}$ B blasts (day 3) **(A)** and $IgM^{+}HEL^{+}$ GC B cells (day 6.5) **(B)**. GC B cells were subdivided as either DZ or LZ cells based on CXCR4 and CD86 expression as shown.

C) Heatmap showing single cell qPCR expression profile of selected targets in B blasts, DZ and LZ SW_{HEL} B cells purified as described in **(A-B)**.

D) Quantification of raw C_T values for γ1-GLT, γ2b-GLT, *Aicda, Bcl6 and Apex1* obtained in **(C)**. Violin plots depict data distribution; each dot represents an individual cell.

E) Pie charts showing quantification of target genes as shown in **(D)**. Numbers indicate the percentage of cells expressing the indicated target.

The limit of detection for analysis was set to 40 cycles, cells with a C_T value < 40 were considered positive events. NTC = no template control. Bulk = bulk population control of 20 cells. Please also see Figure SX.

Figure 4. Expression of GLTs remains low in late GC responses

A) Adoptive transfer protocol of B1-8^{hi} tdTomato (tdT) B cells to investigate the early phases of the immune response to NP-CGG (see STAR methods).

B) Flow cytometric plots showing gating strategy to identify B1-8^{hi} tdT^{+} B cells as shown in (A). Top panel shows representative plots of CD38 vs Fas for donor-derived B1-8^{hi} tdT^{+} B cells and bottom panel the profile for recipient cells in the same mouse.

C) qPCR gene expression profile for γ1-GLT in purified donor-derived B1-8^{hi} tdT^{+} B cells as for **(A-B)**. See (F) for details.

D) Adoptive transfer protocol of B1-8^{hi} tdT^{+} B cells to investigate the late phases of the immune response to NP-GCC. C57BL/6 mice were immunized as shown in **(A)**.

E) Flow cytometric plots showing gating strategy to analyze surface expression of total IgG at day 2 (top panel) and days 4 - 18 (bottom panel) in splenocytes harvested from mice immunized as in **(D)**.

F) qPCR gene expression profile for γ1-GLT in purified donor-derived B1-8^{hi} tdT^{+} B cells as shown in **(D)**. Duplex qPCR analyses were conducted using *Actb* as reference gene. Data is presented as a fold-change compared to day 1.0 B cells (C) or day 4 GC B cells (F) using the $\Delta\Delta C_T$ method. Dots represent individual mice and the black line connects the group medians.

G-H) Flow cytometric quantification of total IgG in donor-derived B1-8^{hi} tdT^{+} cells **(G)** and total numbers of B1-8^{hi} tdT^{+} GC B cells **(H)** in the spleens of C57BL/6 transferred mice identified as in **(D)**. Number of mice used in each time point: day 2 (n=5), day 4 (n=5), day 8 (n=4), day 14 (n=5) and day 18 (n=5). Data is representative of three independent experiments. Total cell numbers were normalized to 1x10^{6} splenocytes. Please also see Figure SX.

Figure 5. Lack of ongoing switching in IgM^{+} B cells from established germinal centers and *in silico* modelling

A) Schematic representation of the clonal and isotype composition of the GCs obtained from the popliteal lymph nodes (pLNs) of PA-GFP mice immunized 15 or 20 days earlier with CGG in alum. Each column represents a single GC and the boxes in each column represent individual clones determined by phylogenetic analysis of single cell mRNA V_H sequences. The size of each box has been scaled to reflect the number of cells in each clone. Grey represents IgG^+ B cells and green represents IgM^+ B cells, as determined by *Igh* mRNA sequences. The boxes outlined in black indicate those selected for the somatic mutation analysis depicted in **(B)**, based on mixed composition by both IgG^+ and IgM^+ cells, and the presence of 4 or more IgM^+ cells.

B) Charts showing clonal trees representing the phylogeny of V_H sequences within B cell clones (symbols according to the legend in the bottom panel).

C) Summary of the data in **(A-B)** showing the SHM content of individual B cells at the time of the inferred switch event (filled red arrowheads). Clones containing only IgM^+ cells (empty red arrowheads) were pooled with those in which switching occurred at the level of the unmutated precursor (zero mutations). For each time point 5 different mice in 3 independent experiments were included.

F-H) Histograms showing distribution of IgG fractions at the end of affinity maturation *in silico* in **(F)** constant switching probability of $p = 0.03$, **(G)** constant switching probability combined with an increased probability of IgG^+ cells to leave the GC and **(H)** dynamic switching with an initial switching probability of $p = 0.15$ and a decaying switching probability of $\gamma = 0.035\ h^{-1}$ (see Fig. 1E). Each distribution shows the fraction of IgG^+ B cells at day 21 after the onset of the GC reaction.

I) Effect of class switch timing on the diversity of Ig-isotypes in simulated GCs. t_{switch} (horizontal axis) denotes the time post GC onset (time post immunization minus 3.5 days) at which CSR is started with a decreasing probability. Each point corresponds to the interquartile range of the IgG fraction among B cells at the end of *in silico* GC reactions in 400 simulations. Please also see Figure SX.

Figure 6. APE1 is downregulated in human GC B cells and its expression is modulated by BCL6

A) Barplot showing expression of human *BCL6, AICDA, UNG, APEX1*, and *APEX2* genes from purified tonsillar naïve B cells and GC B cells by RNA-seq. Data is presented as the log2 fold-change between reads per kilobase per million reads (RPKMs) of GC B cells relative to those on naïve B cells. The bars represent means and error bars ± standard deviations. Dots represent individual donors (n=5).

B) Immunofluorescence images of human tonsil samples showing APE1 (red), IgD (green), and DAPI (blue). Scale bars = 200 μm.

C) Flow cytometric plots showing the gating strategy to purify naïve, DZ and LZ B cells from human tonsils. Activated B cells correspond to naïve B cells stimulated *in vitro* for 72h with IL-21 and CD40L.

D) Immunoblot of human APE1 protein in naïve, DZ, LZ and activated B cells. β-actin was used as a loading control.

E) Quantification of APE1 protein by densitometry as for blot in **(D)**. APE1 expression was normalized using β-actin. Data is presented as a fold-change relative to naïve B cells. Horizontal black bars represent means and dotted grey lines connect samples derived from the same tonsil donor. Numbers on top indicate the respective *p*-value from two-tailed paired t-test analysis, n = 3.

F) Regions where BCL6 binds to the promoter region of the genes encoding for APE1 *(APEX1)*, APE2 *(APEX2)*, BCL6 and TLR1, as determined by ChIP on chip (Ci et al., 2009).

Legend to Supplementary Figures

Figure S1.

A) Gating strategy employed to identify donor-derived SwHEL B cells after adoptive transfer into congenic recipient mice immunized with HEL^{2x}-SRBCs or HEL^{3x}-SRBCs. **B)** Flow cytometric plots showing expression of different markers by responding donor-derived SW_{HEL} GC B cells gated as $CXCR5^{hi}$ $B220^{hi}$ compared to HEL-binding EFPBs identified as $CXCR5^{lo}$ $B220^{lo}$.

Figure S2

A) Dot plot showing raw C_T values for Figure 1E. γ1-GLT, γ2b-GLT, *Bcl6* and *Aicda* expression values are shown together with those for the reference gene *Ubc*. Horizontal grey lines show the C_T mean expression value of *Ubc* across all samples. Dotted grey lines are ± 2 C_T values from *Ubc* C_T mean.
B) Quantification of IgM in EFPBs or GC B cells for samples shown in Fig 2D. Bars represent medians and dots individual mice (n=4). Data is representative of two independent experiments.

Figure S3

A) Flow cytometric plots showing gating strategy used to identify donor-derived SwHEL B cells after immunization with HEL^{3x}. In brief, $CD45.2^+$ recipient mice were adoptively transferred with $CD45.1^+$ SWHEL B cells ($3x10^4$ - $15x10^4$) and simultaneously *i.v.* challenged with $2x10^8$ SRBCs conjugated to HEL^{3x}. Spleens were harvested at the indicated time points to analyze the immune response.
B) qPCR gene expression profile for γ1-GLT. Duplex qPCR analyses were conducted using *Actb* as a reference. Data is expressed as a fold-change compared to day 3.5

mean expression value using the ΔΔCT method. Dots represent the mean of pooled biological replicates (day 0 - 3.5) or individual animals (day 6.5 - 8.5).

C) Dot plot showing raw C_T values for γ1-GLT and the reference gene Actb. Samples were measured in triplicate. Horizontal green and blue lines show the C_T mean value of all samples for γ1-GLT and *Actb*, respectively. Dotted blue lines depict ± 2 C_T values from *Actb* C_T mean. NTC = no template control.

Figure S4

A) Violin plots showing expression levels for the genes *Cxcr4* and *Cd86* by single cell qPCR in activated B cells (day 3) and GC B cells (day 6.5), subdivided as LZ and DZ cells.

B) Pie charts showing quantification of target genes shown in **(A)**. Numbers indicate the percentage of cells expressing the indicated target. Cells with a C_T value < 40 were considered positive. Sample were obtained as shown in Figure 2.

C) Heatmap showing single cell expression of γ1, γ2b, γ2c and γ3-GLTs by qPCR in double positive Foxo1$^+$Myc$^+$ B blast, DZ and LZ GC B cells. Activated B blasts were purified on day 3, whereas GC B cells (both DZ and LZ subsets) were isolated on day 6.5 (see Figure 3 for details).

D) Pie charts showing quantification of γ1- and γ2b-GLT in double positive Foxo1$^+$Myc$^+$ cells as for **(C)**. Numbers indicate the percentage of cells expressing the indicated target. Cells with a C_T value < 40 were considered positive events (see Figure 3E for details).

Figure S5

A) Gating strategy used to identify donor-derived B1-8^{hi} tdT$^+$ B cells after adoptive transfer into congenic recipient mice immunized with NP-CGG (see Figure 4 for details).

B) Dot plot showing raw C_T values for γ1-switch circle transcript (γ1-SWCT) and the reference gene *Actb*. Purified naïve B cells from C57BL/6 wild type mice were stimulated *in vitro* for 24h, 48h and 72h with IL-4 and LPS. Samples were pre-amplified for γ1-SWCT for 22 cycles, and then analyzed by qPCR.

C) Analysis of γ1-SWCT expression as shown in **(B)**. DNA fragments amplified by qPCR were resolved by electrophoresis in a 1.5% agarose gel. NTC = no template control.

Figure S6

A) Charts showing clonal diversity of GCs isolated from popliteal lymph nodes (pLNs) after photoactivation in mice immunized 15 days before with CGG-Alum. Two individual GCs per pLN were photoactivated and separately flow cytometry-sorted, as described (Tas et al., 2016). Pie charts show clonal distribution of sequenced Igh genes in each GC. In the inner ring, each slice represents one distinct clone represented in greyscale, colored slices indicate clones that were found in both GCs (top and bottom pie charts) from the same lymph node. In the outer ring the isotype IgG (black) or IgM (white) of each clone is indicated. Numbers in the center of each chart are the total number of IgM/IgG cells sequenced. Clonal trees represent the phylogeny of IgM heavy-chain variable-segment (V_H) sequences within each clone containing more than 2 cells per clone from pLNs that have more than 5 IgM cells (symbols according to the legend in the top panel). Pairs are from 5 different mice in 3 independent experiments.

D-E) GCs were visualized in the Peyer's patches of unimmunized AID-Cre-Confetti mice. **(D)** Pies of isotype distribution across clones were assembled for single GCs from two separate mice. Inner segments denote clones, outer colored ring denotes isotype. n/n = number of clones/ total number of sequenced cells. **(E)** Clonal trees representing the phylogeny of V_H-segment sequences were constructed from the most

heavily expanded clones containing more than 3 members per clone (grey segments in pies). Symbols correspond to the legend in the lower left panel.

Figure S7

A-B) Same simulation as in Figure 5F with ongoing influx of IgM^+ B cells into the GC. The influx rate decays from 2 cells per hour to zero following a sigmoidal function with half value at day 10 post-GC onset and a width of 10 days.

C-D) Same analysis as in **(A-B)** but, instead of modulating the B cell influx duration, with IgM^+ B cells collecting twice as much antigen per interaction with FDC, which induces more signaling in the subsequent selection steps. In **(A-C)**, the sensitivity of GC reactions to ongoing influx and increased antigen uptake, respectively, is shown with unchanged (p=0.03 per division) switching probability. In **(B-D)** the switching probability was adapted to p=0.05 and p=0.18 per division, respectively, in order to make the simulation consistent with the measured mean IgG dominance. Each graph represents 100 simulation replicates.

Figure S8

ChIP-qPCR analysis of BCL6 in primary B cells using the Nojima culture system. Splenic naïve B cells were magnetically purified and co-cultured for 72 h with Nojima cells supplemented with IL-4. These *in vitro* derived GC (iGC) B cells were flow cytometry purified to assess binding of BCL6 to the γ1-GLT promoter by ChIP-qPCR.

A) Diagram depicting the chromosome location of the γ1-GLT promoter (blue arrow) 2000 bp upstream of the Iγ1 coding sequence (grey segment) in the mouse genome. Green arrows indicate the binding location of the primers used for ChIP-qPCR as shown in **(E)**.

B) Consensus binding motif for BCL6 in murine B cells.

C) Predicted BCL6-binding sites in the γ1-GLT promoter scanned with the JASPAR 2018 database. Yellow and red triangles indicate the location of the predicted sites in the γ1-GLT promoter.

D) Flow cytometric analysis of iGC B cells showing induction of BCL6 after 72h of culture with Nojima cells and IL-4.

E) Bar plot showing enrichment of BCL6 binding across the γ1-GLT promoter in iGC B cells and naïve B cells by ChIP-qPCR. Data was normalized using the percent input method.

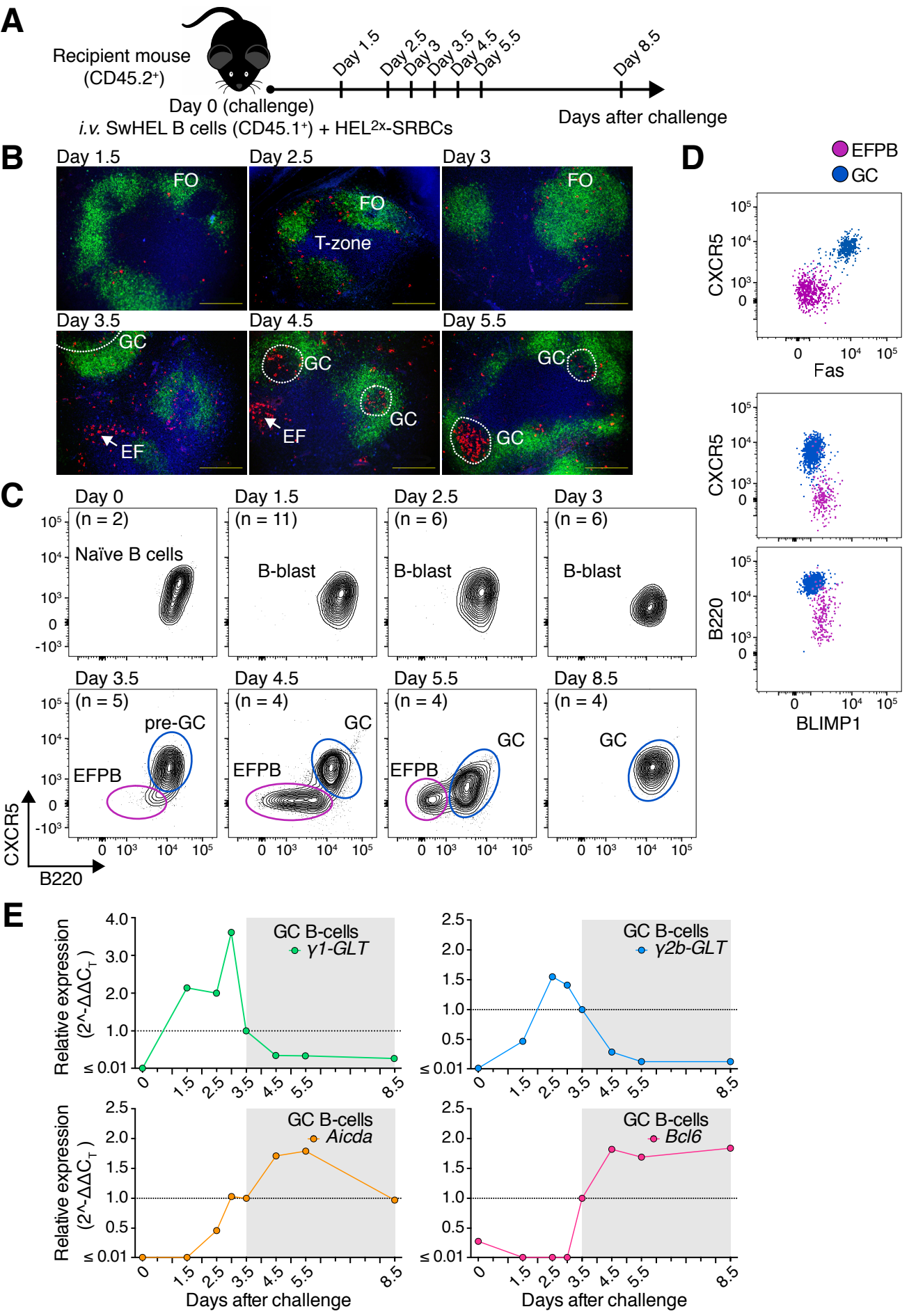
A
Recipient mouse
(CD45.2+)
Day 0 (challenge)
i.v. SwHEL B cells (CD45.1+) + HEL2x-SRBCs
Day 1.5
Day 2.5
Day 3
Day 3.5
Day 4.5
Day 5.5
Day 8.5
Days after challenge
B
Day 1.5
Day 2.5
Day 3
Day 3.5
Day 4.5
Day 5.5
FO
T-zone
GC
EF
C
Day 0
(n = 2)
Naïve B cells
Day 1.5
(n = 11)
B-blast
Day 2.5
(n = 6)
B-blast
Day 3
(n = 6)
B-blast
Day 3.5
(n = 5)
pre-GC
EFPB
Day 4.5
(n = 4)
GC
EFPB
Day 5.5
(n = 4)
GC
EFPB
Day 8.5
(n = 4)
GC
CXCR5
B220
D
EFPB
GC
CXCR5
Fas
CXCR5
B220
BLIMP1
E
Relative expression
(2^-ΔΔCT)
GC B-cells
γ1-GLT
GC B-cells
γ2b-GLT
GC B-cells
Aicda
GC B-cells
Bcl6
Days after challenge
Days after challenge

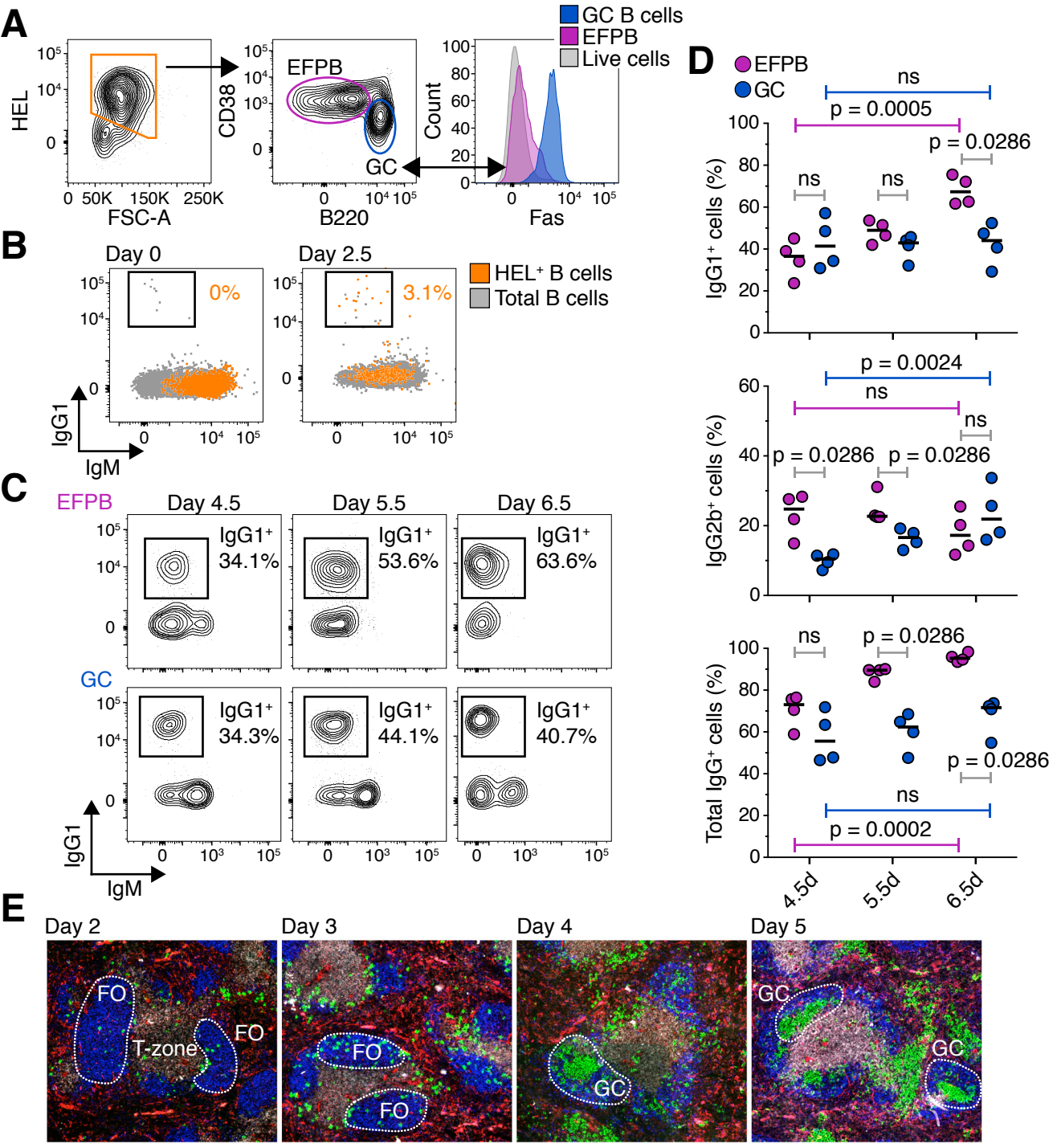
A
GC B cells
EFPB
Live cells
HEL
FSC-A
CD38
B220
EFPB
GC
Count
Fas
B
Day 0
Day 2.5
0%
3.1%
HEL+ B cells
Total B cells
IgG1
IgM
C
EFPB
Day 4.5
Day 5.5
Day 6.5
IgG1+ 34.1%
IgG1+ 53.6%
IgG1+ 63.6%
GC
IgG1+ 34.3%
IgG1+ 44.1%
IgG1+ 40.7%
IgG1
IgM
D
EFPB
GC
IgG1+ cells (%)
p = 0.0005
p = 0.0286
ns
IgG2b+ cells (%)
p = 0.0024
Total IgG+ cells (%)
p = 0.0002
4.5d
5.5d
6.5d
E
Day 2
Day 3
Day 4
Day 5
FO
T-zone
GC

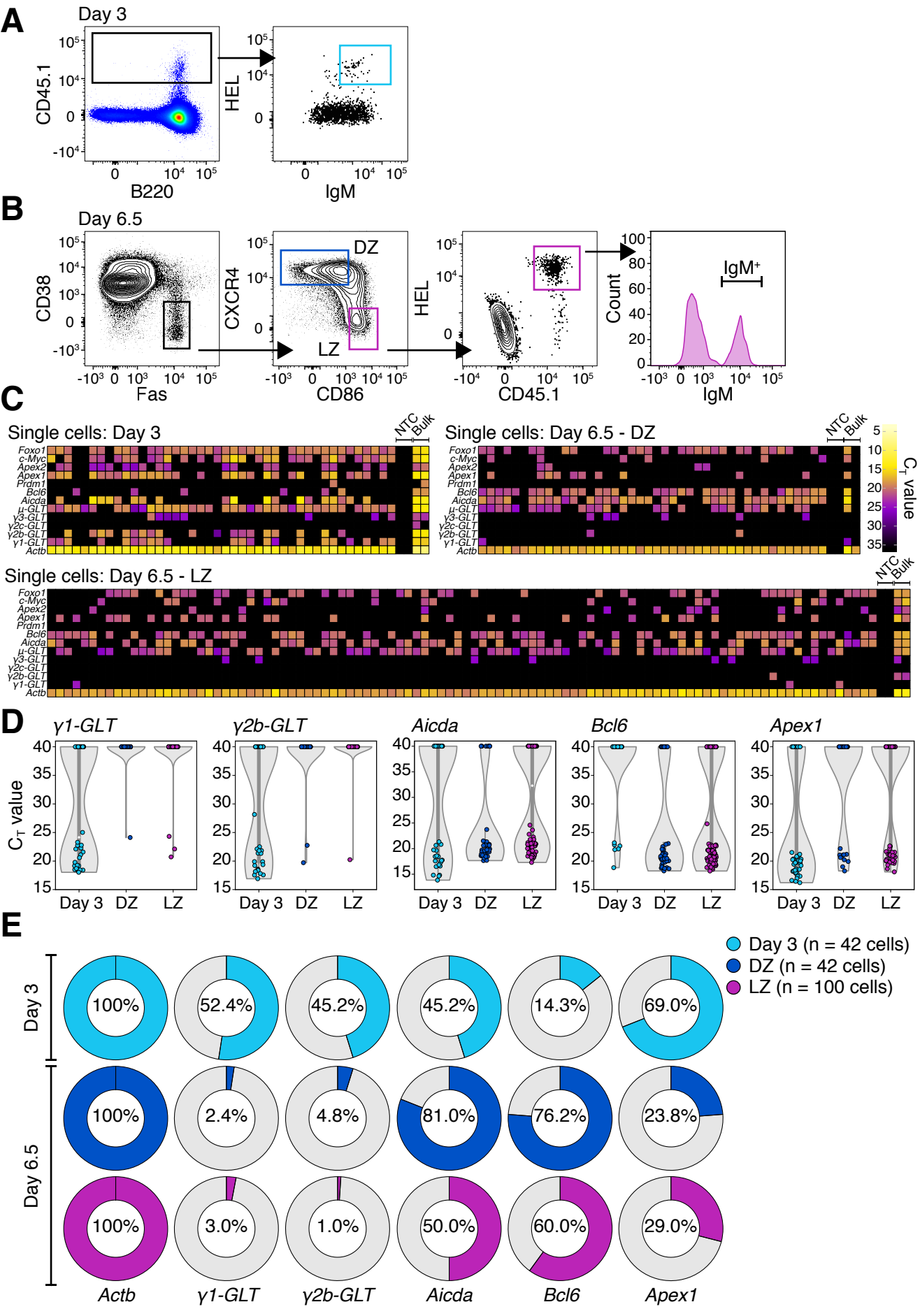
A
Day 3
CD45.1
B220
HEL
IgM
B
Day 6.5
CD38
Fas
CXCR4
CD86
DZ
LZ
HEL
CD45.1
Count
IgM+
IgM
C
Single cells: Day 3
Single cells: Day 6.5 - DZ
Single cells: Day 6.5 - LZ
NTC
Bulk
Foxo1
c-Myc
Apex2
Apex1
Prdm1
Bcl6
Aicda
μ-GLT
γ3-GLT
γ2c-GLT
γ2b-GLT
γ1-GLT
Actb
CT value
D
γ1-GLT
γ2b-GLT
Aicda
Bcl6
Apex1
CT value
Day 3
DZ
LZ
E
Day 3 (n = 42 cells)
DZ (n = 42 cells)
LZ (n = 100 cells)
Day 3
Day 6.5
100%
52.4%
45.2%
45.2%
14.3%
69.0%
100%
2.4%
4.8%
81.0%
76.2%
23.8%
100%
3.0%
1.0%
50.0%
60.0%
29.0%
Actb
γ1-GLT
γ2b-GLT
Aicda
Bcl6
Apex1

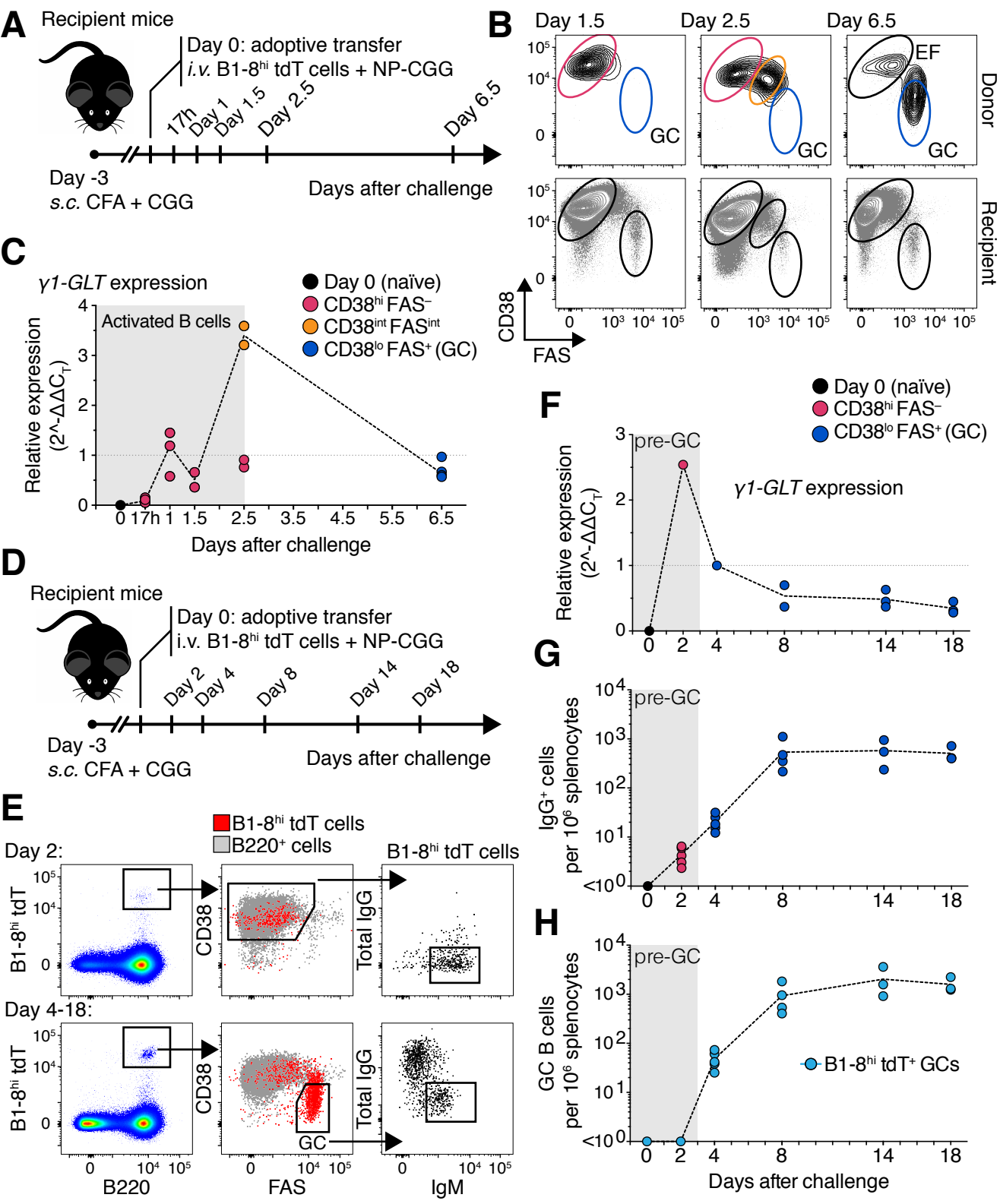
A
Recipient mice
Day 0: adoptive transfer
i.v. B1-8hi tdT cells + NP-CGG
17h
Day 1
Day 1.5
Day 2.5
Day 6.5
Day -3
s.c. CFA + CGG
Days after challenge
B
Day 1.5
Day 2.5
Day 6.5
EF
GC
Donor
Recipient
CD38
FAS
C
γ1-GLT expression
Day 0 (naïve)
CD38hi FAS−
CD38int FASint
CD38lo FAS+ (GC)
Activated B cells
Relative expression
(2^-ΔΔCT)
Days after challenge
D
Recipient mice
Day 0: adoptive transfer
i.v. B1-8hi tdT cells + NP-CGG
Day 2
Day 4
Day 8
Day 14
Day 18
Day -3
s.c. CFA + CGG
Days after challenge
E
B1-8hi tdT cells
B220+ cells
Day 2:
Day 4-18:
B1-8hi tdT
CD38
Total IgG
GC
B220
FAS
IgM
F
Day 0 (naïve)
CD38hi FAS−
CD38lo FAS+ (GC)
pre-GC
γ1-GLT expression
Relative expression
(2^-ΔΔCT)
G
pre-GC
IgG+ cells
per 10^6 splenocytes
H
pre-GC
GC B cells
per 10^6 splenocytes
B1-8hi tdT+ GCs
Days after challenge

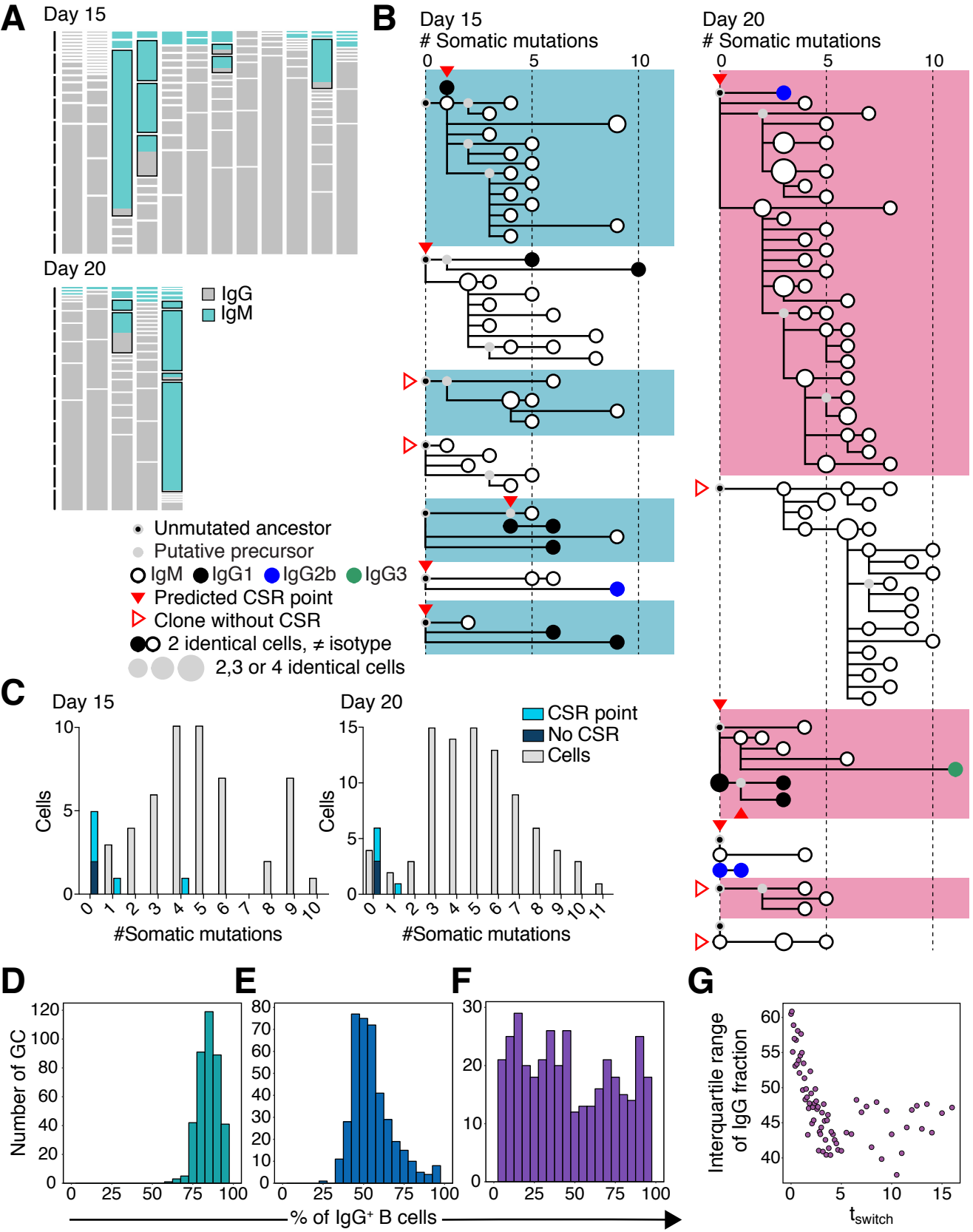
A
Day 15
Day 20
IgG
IgM
B
Day 15
Somatic mutations
Day 20
Somatic mutations
Unmutated ancestor
Putative precursor
IgM IgG1 IgG2b IgG3
Predicted CSR point
Clone without CSR
2 identical cells, ≠ isotype
2,3 or 4 identical cells
C
Day 15
Day 20
CSR point
No CSR
Cells
#Somatic mutations
D
E
F
G
Number of GC
% of IgG+ B cells
Interquartile range of IgG fraction
t switch

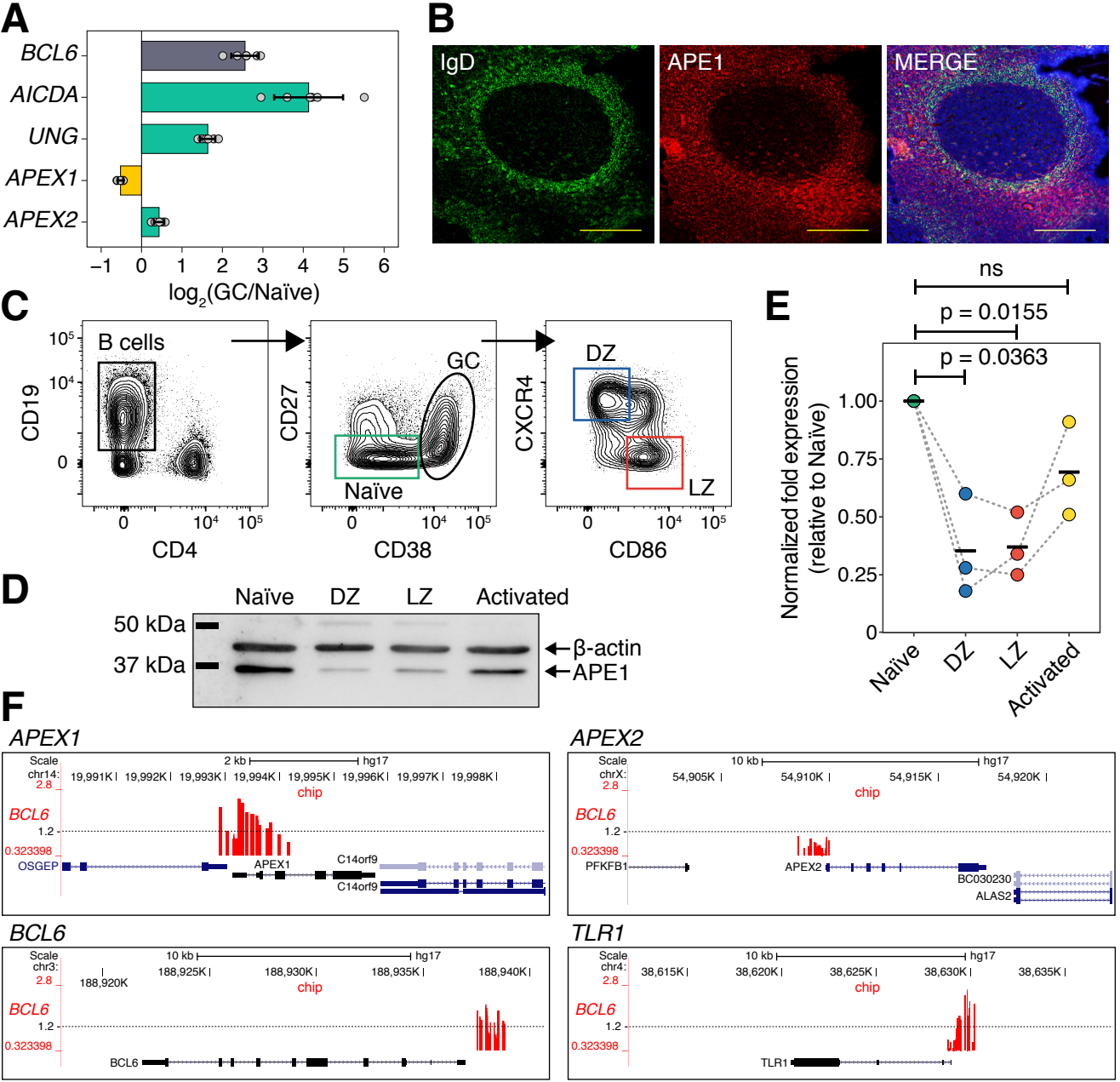
A
BCL6
AICDA
UNG
APEX1
APEX2
−1 0 1 2 3 4 5 6
log2(GC/Naïve)
B
IgD
APE1
MERGE
C
B cells
CD19
CD4
GC
Naïve
CD27
CD38
DZ
LZ
CXCR4
CD86
D
Naïve
DZ
LZ
Activated
50 kDa
37 kDa
β-actin
APE1
E
ns
p = 0.0155
p = 0.0363
Normalized fold expression (relative to Naïve)
1.00
0.75
0.50
0.25
0
Naïve
DZ
LZ
Activated
F
APEX1
Scale
chr14:
2 kb
hg17
19,991K 19,992K 19,993K 19,994K 19,995K 19,996K 19,997K 19,998K
chip
BCL6
2.8
1.2
0.323398
OSGEP
APEX1
C14orf9
C14orf9
APEX2
Scale
chrX:
10 kb
hg17
54,905K 54,910K 54,915K 54,920K
chip
BCL6
PFKFB1
APEX2
BC030230
ALAS2
BCL6
Scale
chr3:
10 kb
hg17
188,920K 188,925K 188,930K 188,935K 188,940K
chip
BCL6
BCL6
TLR1
Scale
chr4:
10 kb
hg17
38,615K 38,620K 38,625K 38,630K 38,635K
chip
BCL6
TLR1

Figure S1

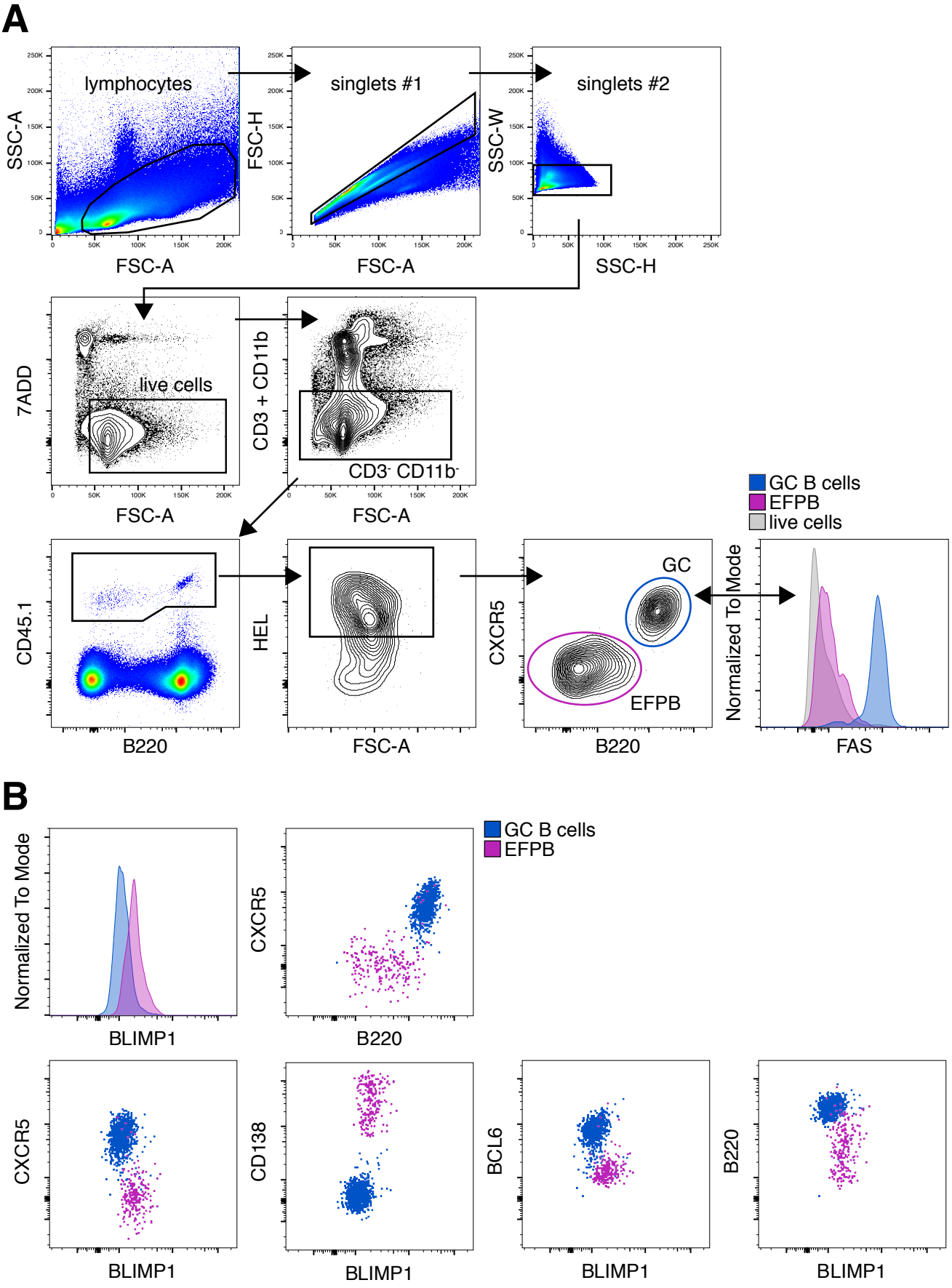
A
lymphocytes
SSC-A
FSC-A
singlets #1
FSC-H
FSC-A
singlets #2
SSC-W
SSC-H
live cells
7ADD
FSC-A
CD3 + CD11b
CD3- CD11b-
FSC-A
GC B cells
EFPB
live cells
CD45.1
B220
HEL
FSC-A
GC
EFPB
CXCR5
B220
Normalized To Mode
FAS
B
Normalized To Mode
BLIMP1
CXCR5
B220
GC B cells
EFPB
CXCR5
BLIMP1
CD138
BLIMP1
BCL6
BLIMP1
B220
BLIMP1

Figure S1. Characterization of donor-derived Sw_{HEL} B cells by flow cytometry. Related to Figure 1.

A) Gating strategy employed to identify donor-derived Sw_{HEL} B cells after adoptive transfer into congenic recipient mice immunized with HEL^{2x}-SRBCs or HEL^{3x}-SRBCs.

B) Flow cytometric plots showing expression of different markers by responding donor-derived SW_{HEL} GC B cells gated as $CXCR5^{hi}$ $B220^{hi}$ compared to HEL-binding EFPBs identified as $CXCR5^{lo}$ $B220^{lo}$.

Figure S2

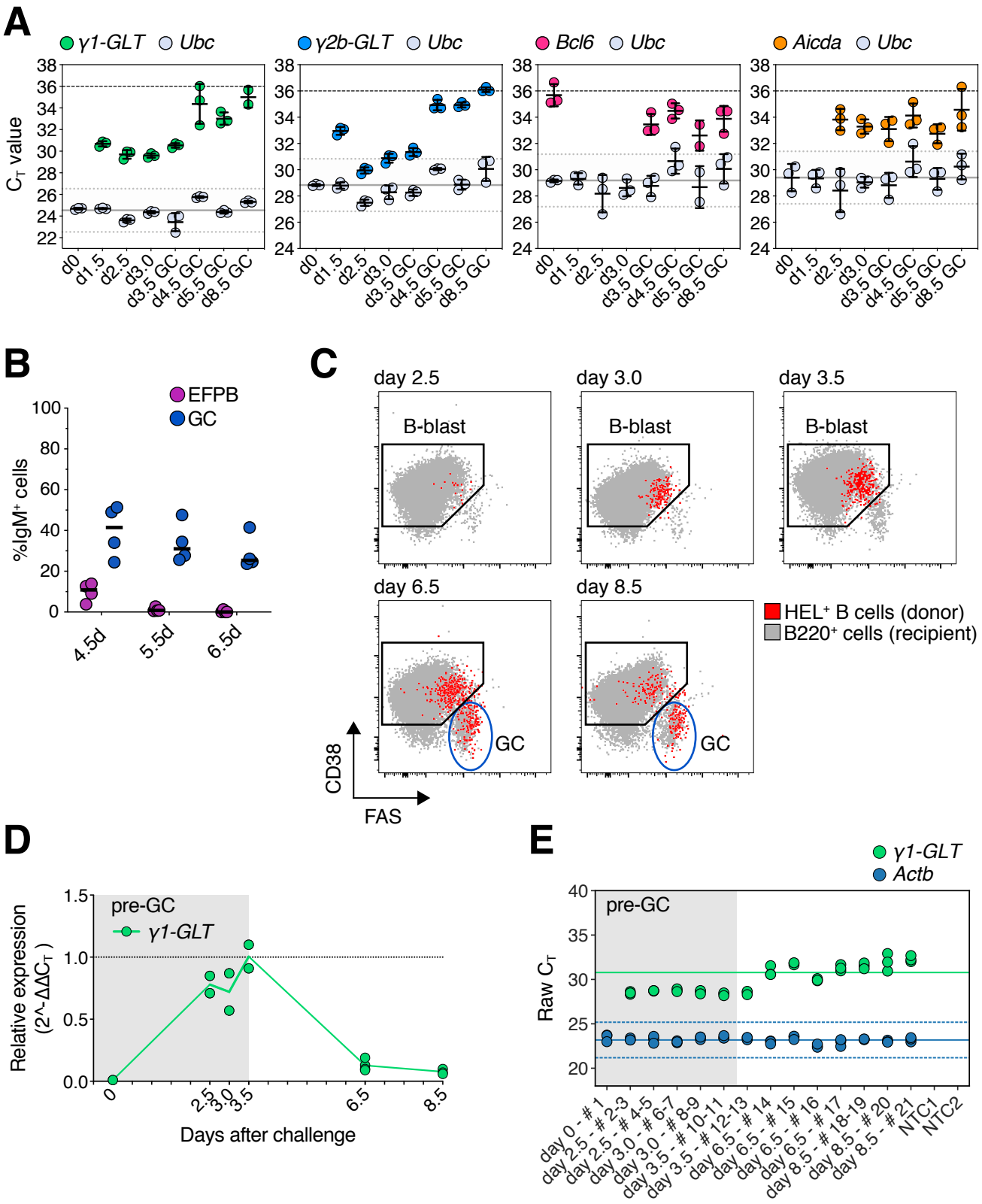
A
γ1-GLT
Ubc
γ2b-GLT
Ubc
Bcl6
Ubc
Aicda
Ubc
C_T value
d0
d1.5
d2.5
d3.0
d3.5 GC
d4.5 GC
d5.5 GC
d8.5 GC
B
EFPB
GC
%IgM+ cells
4.5d
5.5d
6.5d
C
day 2.5
day 3.0
day 3.5
day 6.5
day 8.5
B-blast
GC
CD38
FAS
HEL+ B cells (donor)
B220+ cells (recipient)
D
pre-GC
γ1-GLT
Relative expression
(2^-ΔΔC_T)
Days after challenge
E
γ1-GLT
Actb
pre-GC
Raw C_T
day 0 - # 1
day 2.5 - # 2-3
day 2.5 - # 4-5
day 3.0 - # 6-7
day 3.0 - # 8-9
day 3.5 - # 10-11
day 3.5 - # 12-13
day 6.5 - # 14
day 6.5 - # 15
day 6.5 - # 16
day 6.5 - # 17
day 8.5 - # 18-19
day 8.5 - # 20
day 8.5 - # 21
NTC1
NTC2

Figure S2. Raw gene expression profiles and quantification of surface IgM in Sw_{HEL} B cells, and analysis of CSR upon immunization with HEL^{3x}-SRBCs. Related to Figure 1 and Figure 2.

A) Dot plot showing raw C_T values for Figure 1E. *γ1-GLT, γ2b-GLT*, *Bcl6* and *Aicda* expression values are shown together with those for the reference gene *Ubc*. Horizontal grey lines show the C_T mean expression value of *Ubc* across all samples. Dotted grey lines are ± 2 C_T values from *Ubc* C_T mean.

B) Quantification of IgM in EFPBs or GC B cells for samples shown in Fig 2D. Bars represent medians and dots individual mice (n=4). Data is representative of two independent experiments.

C) Flow cytometric plots showing gating strategy used to identify donor-derived Sw_{HEL} B cells after immunization with HEL^{3x}. In brief, $CD45.2^+$ recipient mice were adoptively transferred with $CD45.1^+$ SW_{HEL} B cells ($3x10^4$ - $15x10^4$) and simultaneously *i.v.* challenged with $2x10^8$ SRBCs conjugated to HEL^{3x}. Spleens were harvested at the indicated time points to analyze the immune response.

D) qPCR gene expression profile for *γ1-GLT*. Duplex qPCR analyses were conducted using *Actb* as a reference. Data is expressed as a fold-change compared to day 3.5 mean expression value using the ΔΔCT method. Dots represent the mean of pooled biological replicates (day 0 - 3.5) or individual animals (day 6.5 - 8.5). n = 4 mice per timepoint.

E) Dot plot showing raw C_T values for *γ1-GLT* and the reference gene *Actb*. Samples were measured in triplicate. Horizontal green and blue lines show the C_T mean value across all samples for *γ1-GLT* and *Actb*, respectively. Dotted blue lines depict ± 2 C_T values from *Actb* C_T mean. NTC = no template control.

Figure S3

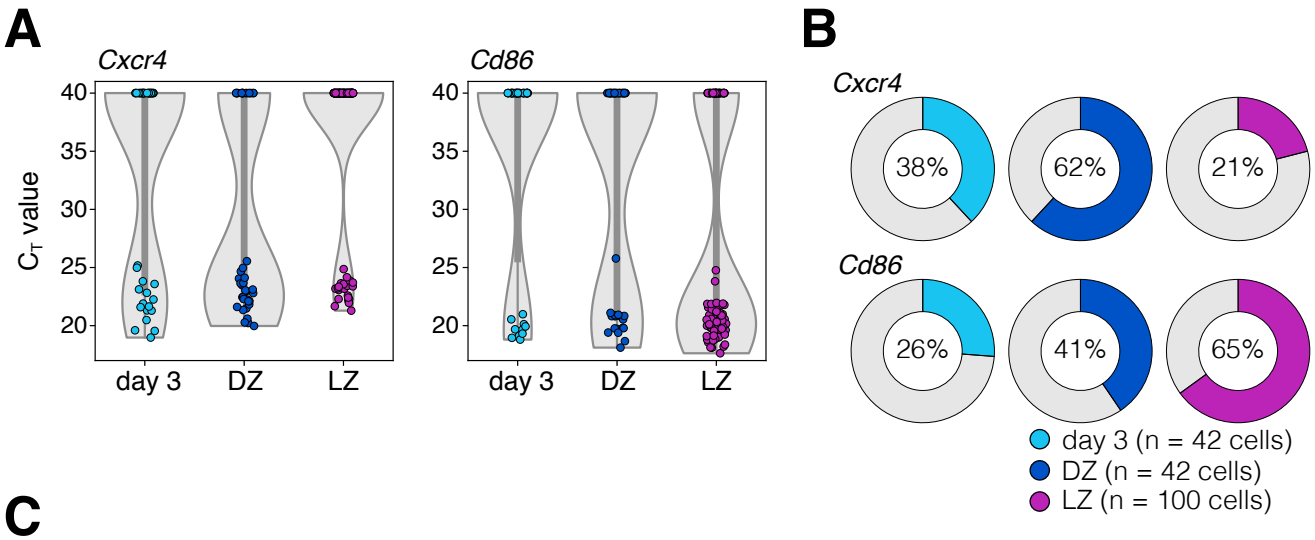
A
Cxcr4
Cd86
C_T value
40
35
30
25
20
day 3
DZ
LZ
B
Cxcr4
38%
62%
21%
Cd86
26%
41%
65%
day 3 (n = 42 cells)
DZ (n = 42 cells)
LZ (n = 100 cells)

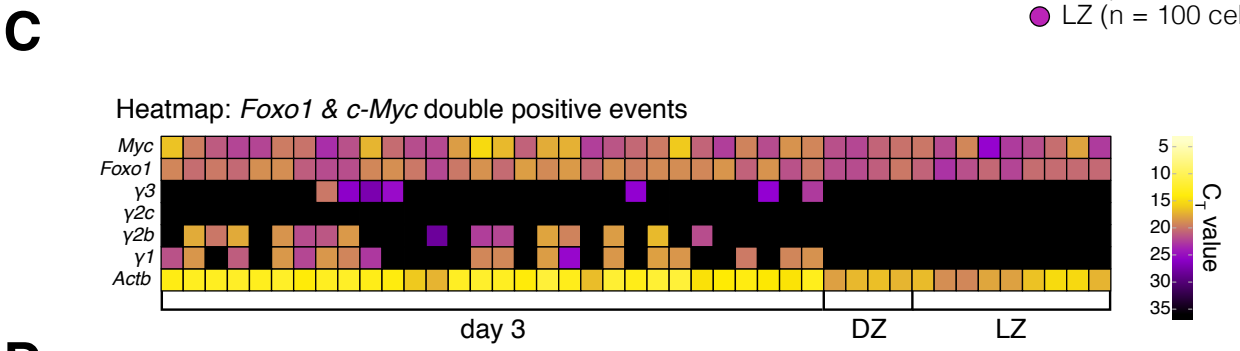
C
Heatmap: Foxo1 & c-Myc double positive events
Myc
Foxo1
γ3
γ2c
γ2b
γ1
Actb
day 3
DZ
LZ
5
10
15
20
25
30
35
C_T value

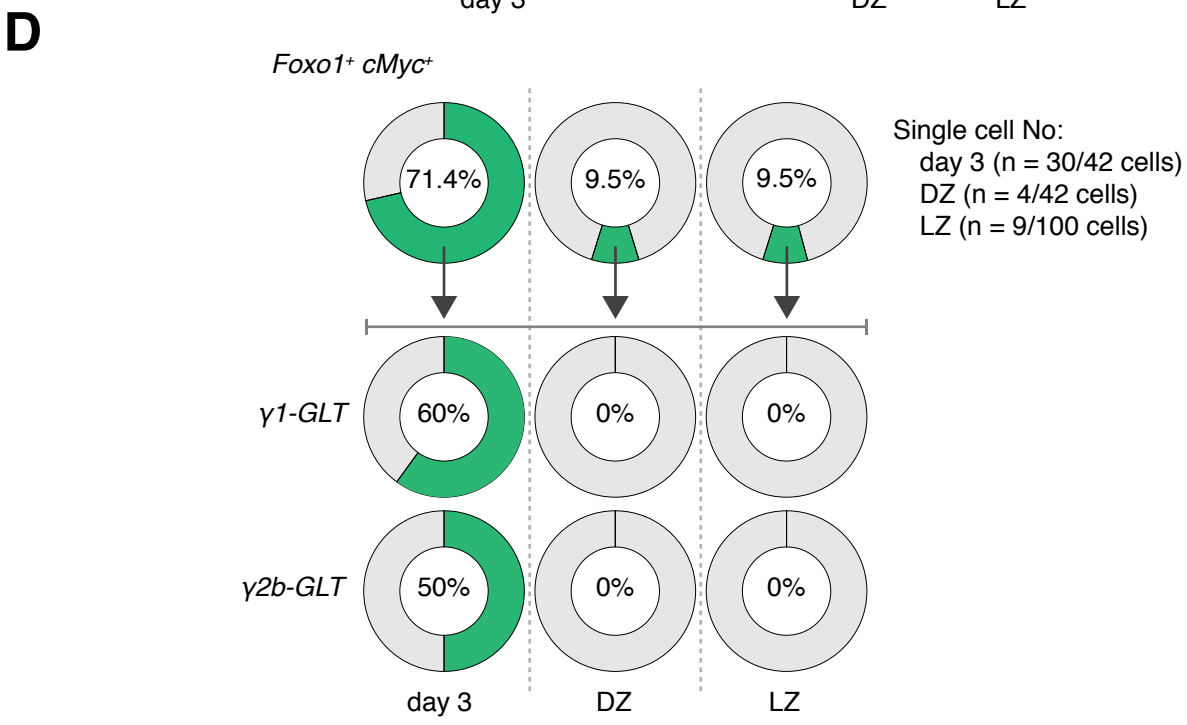
D
Foxo1⁺ cMyc⁺
71.4%
9.5%
9.5%
Single cell No:
day 3 (n = 30/42 cells)
DZ (n = 4/42 cells)
LZ (n = 9/100 cells)
γ1-GLT
60%
0%
0%
γ2b-GLT
50%
0%
0%
day 3
DZ
LZ

Figure S3. *Cxrc4* and *Cd86* gene expression in SwHEL B cells and GLT expression analysis in *Foxo1*$^{+}$ *c-Myc*$^{+}$ SwHEL B cells. Related to Figure 3.

A) Violin plots showing *Cxcr4* and *Cd86* gene expression in the indicated subsets by single cell qPCR.

B) Pie charts showing quantification of target genes as shown in **(A)**.

C) Heatmap showing single cell expression of *γ-GLTs* by qPCR in double positive *Foxo1*$^{+}$*Myc*$^{+}$ B blast, DZ and LZ GC B cells (see Figure 3 for details).

D) Pie charts showing quantification of *γ1-* and *γ2b-GLT* in double positive *Foxo1*$^{+}$*Myc*$^{+}$ cells as for **(C)**.

In pie charts (B and D), numbers indicate the percentage of cells expressing the indicated target. Cells with a C_T value < 40 were considered positive events (see Figure 3 for details).

Figure S4

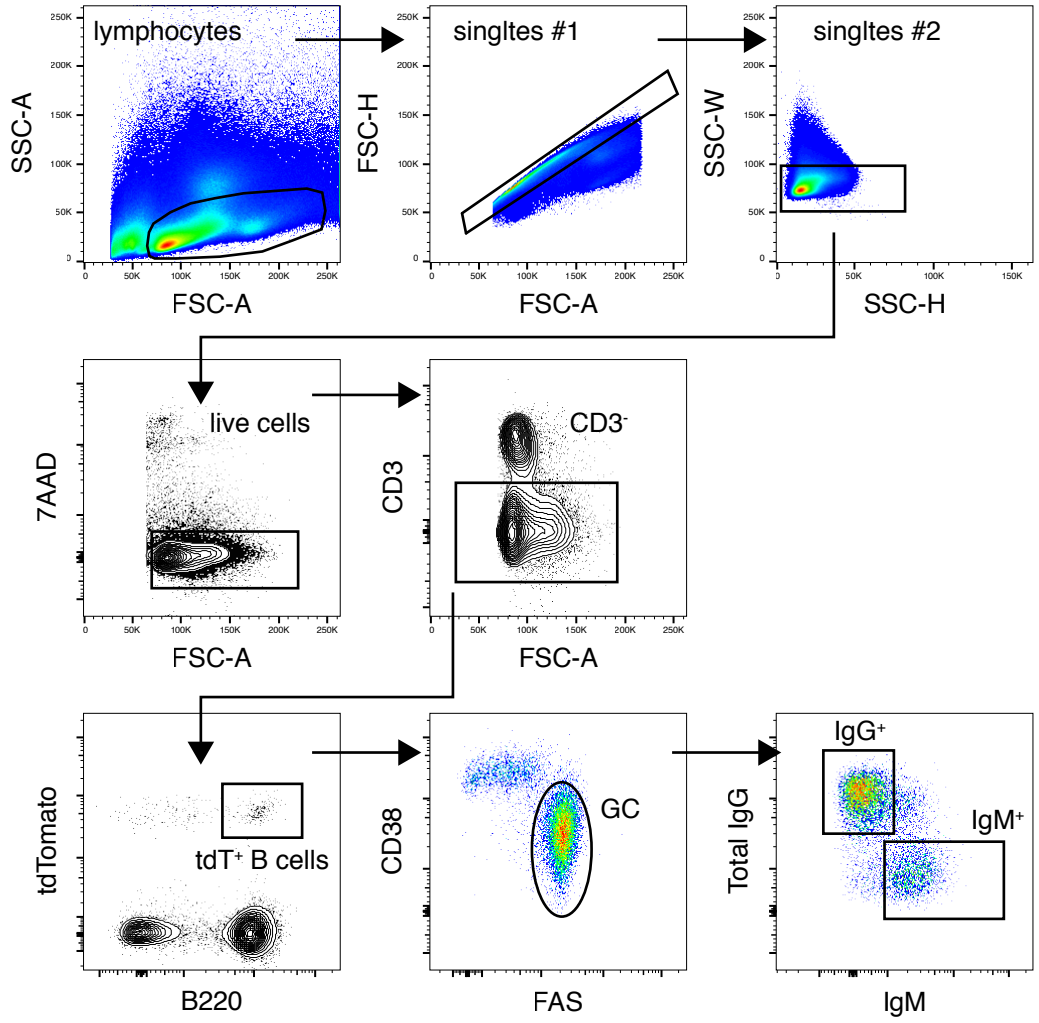
A
lymphocytes
SSC-A
FSC-A
singltes #1
FSC-H
FSC-A
singltes #2
SSC-W
SSC-H
live cells
7AAD
FSC-A
CD3⁻
CD3
FSC-A
tdT⁺ B cells
tdTomato
B220
GC
CD38
FAS
IgG⁺
IgM⁺
Total IgG
IgM

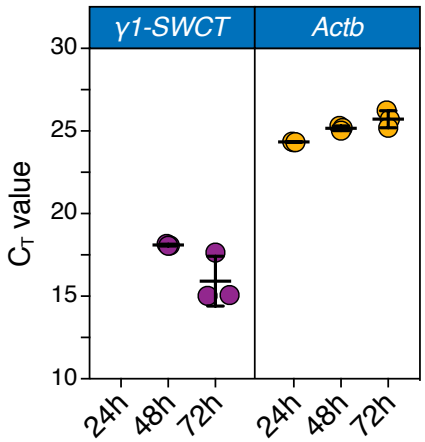
B
γ1-SWCT
Actb
C_T value
30
25
20
15
10
24h
48h
72h
24h
48h
72h

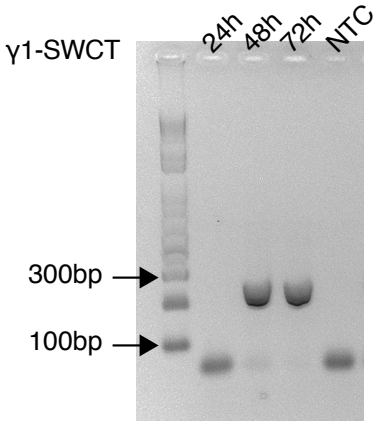
C
γ1-SWCT
24h
48h
72h
NTC
300bp
100bp

Figure S4. Characterization of B1-8^{hi} tdT^{+} B cells and *in-vitro* analysis of switch circle transcript formation. Related to Figure 4.

A) Gating strategy used to identify donor-derived B1-8^{hi} tdT^{+} B cells after adoptive transfer into congenic recipient mice immunized with NP-CGG (see Figure 4 for details).

B) Dot plot showing raw C_T values for γ1-switch circle transcript (γ1-SWCT) and the reference gene *Actb*. Purified naïve B cells from C57BL/6 wild type mice were stimulated *in vitro* for 24h, 48h and 72h with IL-4 and LPS. Samples were pre-amplified for γ1-SWCT for 22 cycles, and then analyzed by qPCR.

C) Analysis of γ1-SWCT expression as shown in **(B)**. DNA fragments amplified by qPCR were resolved by electrophoresis in a 1.5% agarose gel. NTC = no template control.

Figure S5

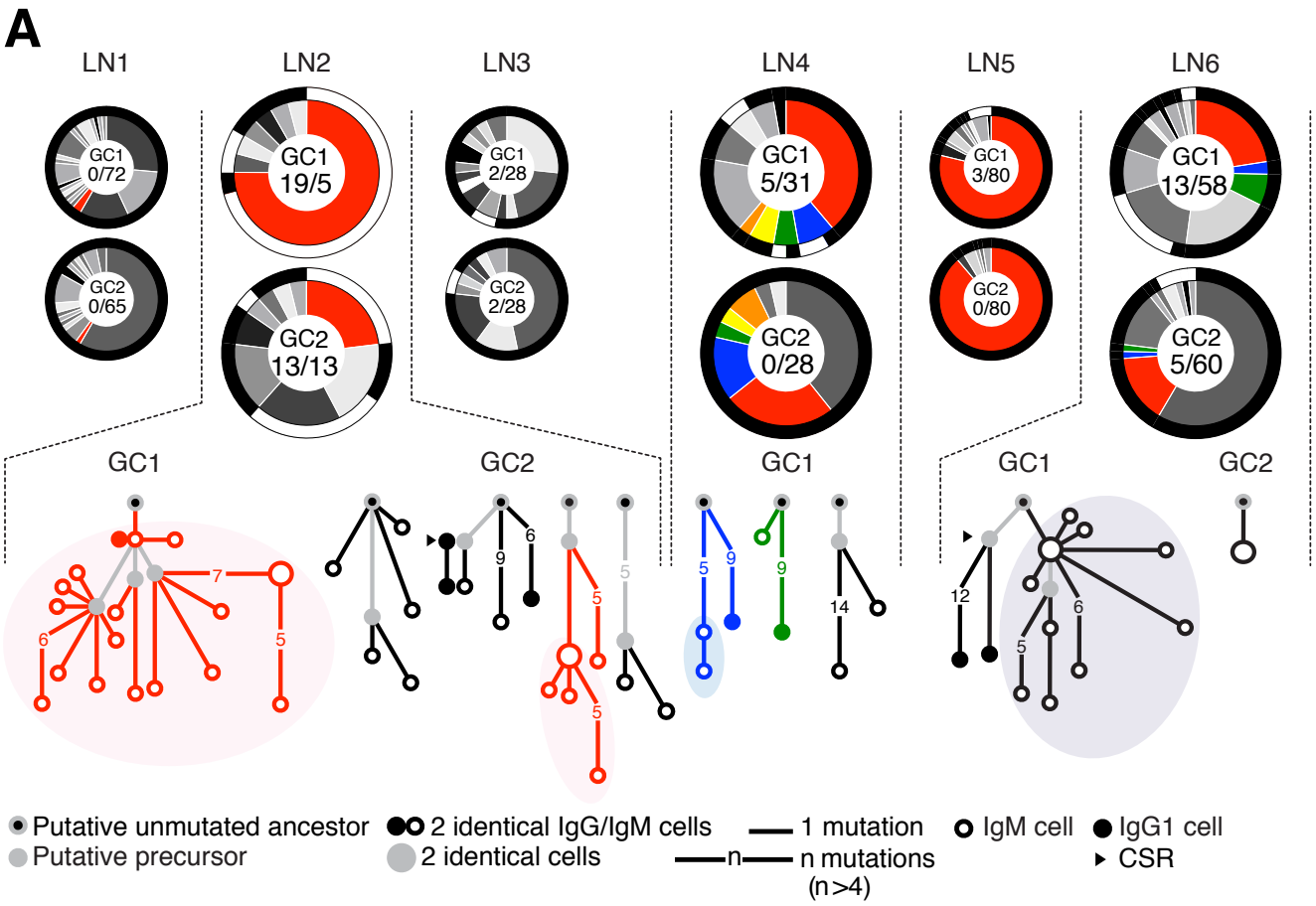
A
LN1
LN2
LN3
LN4
LN5
LN6
GC1 0/72
GC2 0/65
GC1 19/5
GC2 13/13
GC1 2/28
GC2 2/28
GC1 5/31
GC2 0/28
GC1 3/80
GC2 0/80
GC1 13/58
GC2 5/60
GC1
GC2
GC1
GC1
GC2
Putative unmutated ancestor
Putative precursor
2 identical IgG/IgM cells
2 identical cells
1 mutation
n mutations (n>4)
IgM cell
IgG1 cell
CSR

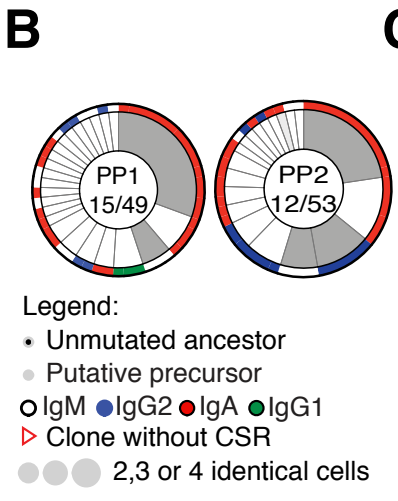
B
PP1 15/49
PP2 12/53
Legend:
Unmutated ancestor
Putative precursor
IgM IgG2 IgA IgG1
Clone without CSR
2,3 or 4 identical cells

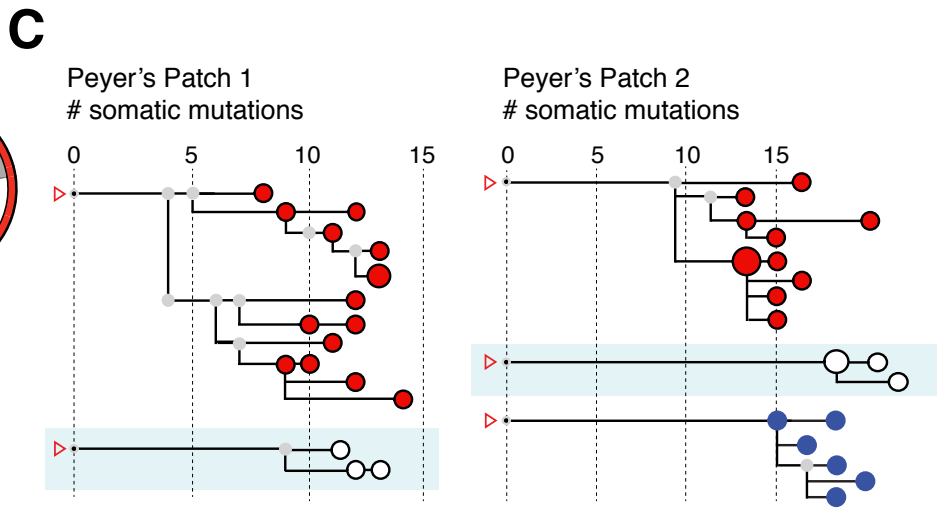
C
Peyer's Patch 1
somatic mutations
Peyer's Patch 2
somatic mutations
0
5
10
15

Figure S5. Clonal analysis of photoconverted GC B cells in lymph nodes and Peyer's Patches. Related to Figure 5.

A) Charts showing clonal diversity of GCs isolated from popliteal lymph nodes (pLNs) after photoactivation in mice immunized 15 days before with CGG-Alum. Two individual GCs per pLN were photoactivated and separately flow cytometry-sorted, as described (Tas et al., 2016). Pie charts show clonal distribution of sequenced Igh genes in each GC. In the inner ring, each slice represents one distinct clone represented in greyscale, colored slices indicate clones that were found in both GCs (top and bottom pie charts) from the same lymph node. In the outer ring the isotype IgG (black) or IgM (white) of each clone is indicated. Numbers in the center of each chart are the total number of IgM-/IgG cells sequenced. Clonal trees represent the phylogeny of IgM heavy-chain variable-segment (V_H) sequences within each clone containing more than 2 cells per clone from pLNs that have more than 5 IgM cells (symbols according to the legend in the top panel). Pairs are from 5 different mice in 3 independent experiments.

B-C) GCs were visualized in the Peyer's patches of unimmunized AID-Cre-Confetti mice. **(B)** Pies of isotype distribution across clones were assembled for single GCs from two separate mice. Inner segments denote clones, outer colored ring denotes isotype. n/n = number of clones/ total number of sequenced cells. **(C)** Clonal trees representing the phylogeny of V_H-segment sequences were constructed from the most heavily expanded clones containing more than 3 members per clone (grey segments in pies). Symbols correspond to the legend in the lower left panel.

Figure S6

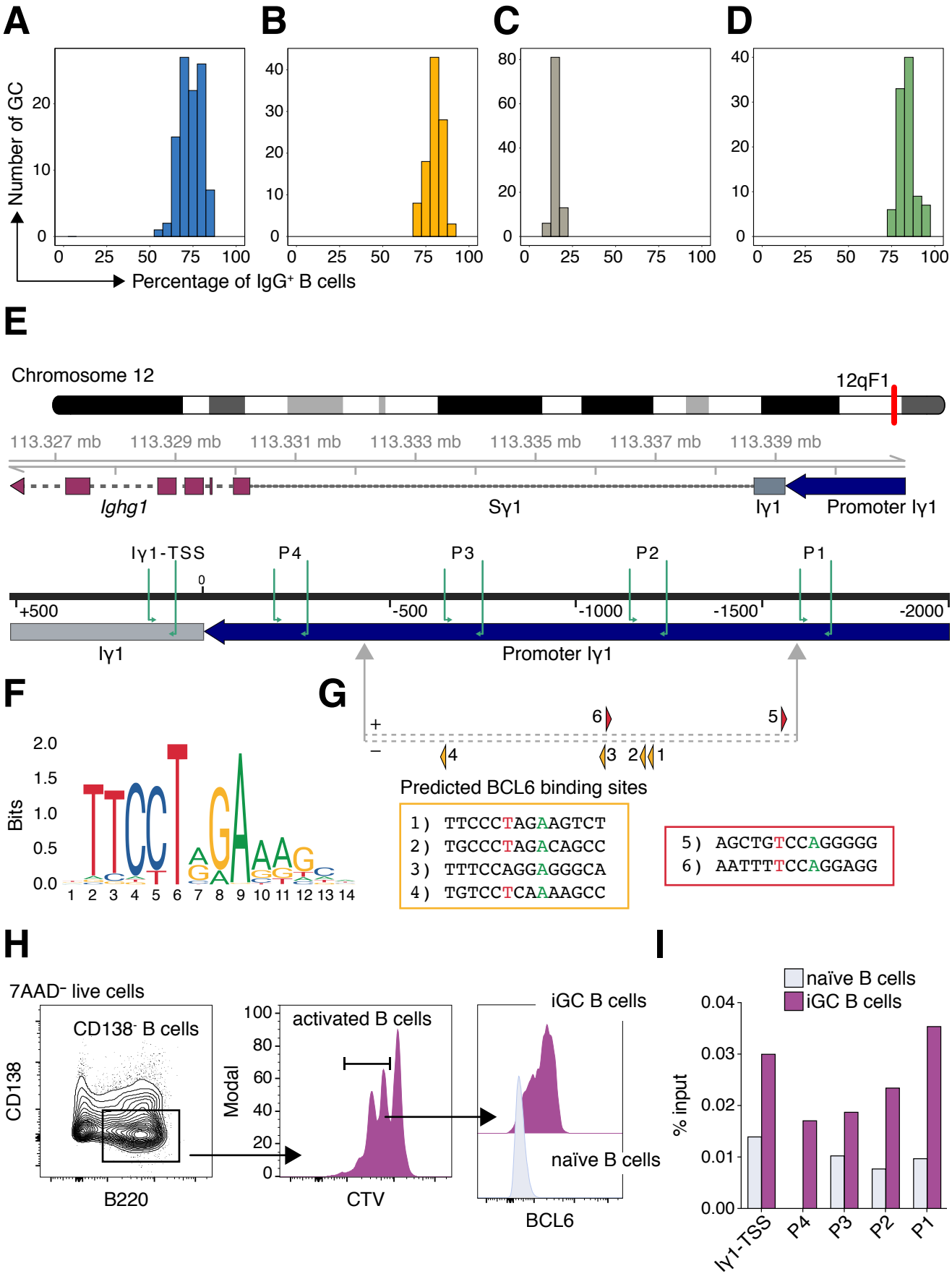
A
B
C
D
Number of GC
Percentage of IgG+ B cells
E
Chromosome 12
12qF1
113.327 mb
113.329 mb
113.331 mb
113.333 mb
113.335 mb
113.337 mb
113.339 mb
Ighg1
Sγ1
Iγ1
Promoter Iγ1
Iγ1-TSS
P4
P3
P2
P1
+500
-500
-1000
-1500
-2000
F
Bits
G
Predicted BCL6 binding sites
1) TTCCCTAGAAGTCT
2) TGCCCTAGACAGCC
3) TTTCCAGGAGGGCA
4) TGTCCTCAAAAGCC
5) AGCTGTCCAGGGGG
6) AATTTTCCAGGAGG
H
7AAD- live cells
CD138- B cells
CD138
B220
activated B cells
Modal
CTV
iGC B cells
naïve B cells
BCL6
I
naïve B cells
iGC B cells
% input

Figure S6. Mathematical modelling and ChIP-qPCR analysis of BCL6 in primary B cells. Related to Figure 5 and Figure 6.

A-B) Same simulation as in Figure 5F with ongoing influx of IgM^+ B cells into the GC. The influx rate decays from 2 cells per hour to zero following a sigmoidal function with half value at day 10 post-GC onset and a width of 10 days.

C-D) Same analysis as in **(A-B)** but, instead of modulating the B cell influx duration, with IgM^+ B cells collecting twice as much antigen per interaction with FDC, which induces more signaling in the subsequent selection steps. In **(A-C)**, the sensitivity of GC reactions to ongoing influx and increased antigen uptake, respectively, is shown with unchanged (p=0.03 per division) switching probability. In **(B-D)** the switching probability was adapted to p=0.05 and p=0.18 per division, respectively, in order to make the simulation consistent with the measured mean IgG dominance. Each graph represents 100 simulation replicates.

E-I) ChIP-qPCR analysis of BCL6 in primary B cells using the Nojima culture system. Splenic naïve B cells were magnetically purified and co-cultured for 72 h with Nojima cells supplemented with IL-4. These *in vitro* derived GC (iGC) B cells were flow cytometry purified to assess binding of BCL6 to the *γ1-GLT* promoter by ChIP-qPCR.

E) Diagram depicting the chromosome location of the *γ1-GLT* promoter (blue arrow) 2000 bp upstream of the Iγ1 coding sequence (grey segment) in the mouse genome. Green arrows indicate the binding location of the primers used for ChIP-qPCR as shown in **(I)**.

F) Consensus binding motif for BCL6 in murine B cells.

G) Predicted BCL6-binding sites in the *γ1-GLT* promoter scanned with the JASPAR 2018 database. Yellow and red triangles indicate the location of the predicted sites in the *γ1-GLT* promoter.

H) Flow cytometric analysis of iGC B cells showing induction of BCL6 after 72h of culture with Nojima cells and IL-4.

I) Bar plot showing enrichment of BCL6 binding across the *γ1-GLT* promoter in iGC B cells and naïve B cells by ChIP-qPCR. Data was normalized using the percent input method. Data is representative of three independent experiments.

Table S1. Sequences of primers and probes used to detect GLT and *Actb* expression by qPCR. Related to Figure 1, 3 and 4.

Target	Primer Sequence (5' - 3')	Probe Sequence (5' - 3')
γ1-GLT	F: CGAGAAGCCTGAGGAATGTGT R: GGAGTTAGTTTGGGCAGCAGAT	FAM-TGGTTCTCTCAACCTGTAGTCCATGCCA
γ2b-GLT	F: CGCACACCTACAGACAACCAG R: GTCACAGAGGAACCAGTTGTATC	FAM-CCAGGGGGCCAGTGGATAGACTGAT
γ2c-GLT	F: GGACCACTAAAGCTGCTGACACAT R: AACCCTTGACCAGGCATCCT	FAM-AGCCCCATCGGTCTATCCACTGGC
γ3-GLT	F: GACCAAATTCGCTGAGTCATCA R: ACCGAGGATCCAGATGTGTCA	FAM-CTGTCTATCCCTTGGTCCCTGGCTGC
μ-GLT	F: TCTGGACCTCTCCGAAACCA R: ATGGCCACCAGATTCTTATCAGA	FAM-ATGTCTTCCCCCTCGTCTCCTGCG
Actb	F: CGTGAAAAGATGACCCAGATCA R: TGGTACGACCAGAGGCATACAG	HEX-TCAACACCCCAGCCATGTACGTAGCC

Table S2. Sequences of primers used in ChIP-qPCR studies. Related to STAR Methods.

Target	Forward Primer	Reverse Primer
Iγ1-P1	5‘-GCTCCACCTACCTTGTCTTTAT-3’	5’-GAGATGGGTTCAGAGTGTCATAG-3’
Iγ1-P2	5’-CACTCTCACTCCAGGGTATAGA-3’	5’-TGAGACCCAGAACACAGAATTAG-3’
Iγ1-P3	5’-CTCCCACAACCTGTACCTAAAT-3’	5’-GGACATGGAAGTAGAGGATCAAA-3’
Iγ1-P4	5’-GTCAGGAAAGAGTGGGCATAA-3’	5’-CTGGCTGTACTCCTGTTTCTC-3’
Iγ1-TSS	5’-GGGCAGGACCAAAACAGGAA-3’	5’-TTTCCCTGCTGACCCCACTC-3’